## Title

Lateral Control of Heavy Duty Vehicles for Automated Highway System: Experimental Study on a Tractor Semi-trailer



## Authors

Hingwe, Pushkar
Wang, Jeng-Yu
Tai, Meihua
et al.

## Publication Date

2000

CALIFORNIA PATH PROGRAM
INSTITUTE OF TRANSPORTATION STUDIES
UNIVERSITY OF CALIFORNIA, BERKELEY

# Lateral Control of Heavy Duty Vehicles for Automated Highway System: Experimental Study on a Tractor Semi-trailer

**Pushkar Hingwe, Jeng-Yu Wang,**
**Meihua Tai, Masayoshi Tomizuka**
*University of California, Berkeley*

**California PATH Working Paper**
**UCB-ITS-PWP-2000-1**

This work was performed as part of the California PATH Program of the University of California, in cooperation with the State of California Business, Transportation, and Housing Agency, Department of Transportation; and the United States Department Transportation, Federal Highway Administration.



Report for MOU 313

January 2000

ISSN 1055-1417

PROJECT TITLE:

# Lateral Control of Heavy Duty Vehicles for Automated Highway System: Experimental Study on a Tractor Semi-trailer

By
Pushkar Hingwe
Jeng-Yu Wang
Meihua Tai
Masayoshi Tomizuka

Department of Mechanical Engineering
University of California Berkeley
Berkeley CA 94709

Annual report for the first year of MOU 313

March 1999

## Executive Summary

The project "Lateral Control of Heavy Duty Vehicles for Automated Highway Systems" (MOU 313) represents continuation of the heavy vehicle research in PATH which was initiated in 1993 with MOU 129, "Steering and Braking Control of Heavy Duty Vehicles" and was followed with MOU 242, "Steering and Braking Control of Heavy Duty Vehicles". While the emphasis of the earlier projects was on analysis of lateral control for heavy vehicles, namely, model development and control design, the emphasis of MOU 313, has been experimental evaluation of the models and the controllers developed so far.

A class eight truck and a 45 feet long trailer have been instrumented for the purpose of lateral and longitudinal control. Steering actuator was developed and installed on the pre-existing steering system. Software to control the steering actuator has been coded and tested. For differential brake control, actuators have been developed and installed on the vehicle. Magnetometer arrays to measure the lateral displacement of the vehicle from the road center line have been installed. A new processing algorithm for magnetometer outputs was developed to extend the range of the existing magnetic sensing scheme used in PATH. This scheme has become standard in other PATH projects as well. Inertial sensors such as accelerometers and gyroscopes have been installed on the tractor and the trailer. String Potentiometers measure the articulation angle and the road wheel angle. The sensors and actuators have been interfaced to the A/D and D/A board by a generic interface board which can be potentially used for future PATH applications.

Linear and nonlinear controllers were designed and tuned for the test vehicle. Specifically, an $H_\infty$ loop shaping controller was designed. This was compared with a classical loop shaping controller. Sliding Mode Controller (SMC) is known for its robust performance in presence of parametric uncertainties and bounded disturbances. An SMC controller was designed and evaluated by simulation.

Open-loop experiments were carried out to study the dynamics of the vehicle system and estimate system parameters. A linear model was tuned to show a close match between the model and the experimental data. The linear controllers were tested in closed loop experiments at Crow's Landing test facility. Automated lane following was achieved with good performance (smooth steering action and moderate tracking errors) for speeds up to 45 miles per hour on curves and up to 60 miles per hour on straight sections.

The success of preliminary designs has given PATH the confidence to conduct testing on differential braking. In the remaining year of the project, we aim to achieve hands off operation at highway speeds and use differential braking for performance enhancement of the lateral control.

## Abstract

This report presents achievements of the MOU 313. "Lateral Control of Heavy Duty Vehicles for Automated Highway Systems" in the year 1998-1999. The goal of the project is to demonstrate lane following by automatic steering for tractor semi-trailer vehicles. Towards this goal, a class eight truck and a 45 feet long trailer were instrumented. The hardware development was a major effort in this year and is presented in detail. The actuators installed for lateral control were steering for and brake actuators. The open loop response of the steering actuator was studied in frequency domain. Based on this response, a minor loop controller is designed for the steering actuator loop. Accelerometers and gyroscopes were installed on the vehicle. The acceleration and yaw response of the vehicle to the road wheel angle was studied in a series of open loop tests. The results of the open loop tests are presented. Previous PATH research (1993-1996) has resulted in the design of several nonlinear controllers for lateral control of heavy vehicles. Nevertheless, from the point of view of preliminary implementation, two linear controllers, one based on classical loop shaping and the other based on optimal $H_\infty$ loop shaping were designed. In addition, a nonlinear Sliding Mode Control for robustness to parametric and model uncertainties was designed. Experimental implementation of the linear controller was accomplished last year for speeds up to 45mph. Results of this experiment are presented.

Key Words: Commercial Heavy Vehicles, lateral control, H-infinity control, Sliding Mode Control, Experimental evaluation

## 1 Introduction:

The importance of commercial vehicles as the primary candidate for deployment of automated driving is being acknowledged in recent years and research on heavy vehicles is becoming an active area. The Federal Highway Administration's (FHWA's) WesTrack facility in Nevada and research by a group in Eindhoven University of Technology, Netherlands- studying automated control of articulated commuter buses- are examples of increasing attention to this field. Reasons for interest in heavy vehicles include: (a) operation of commercial vehicles is profit oriented, and the reduced operating cost along with faster and more reliable operation make automated driving appealing; (b) the driver stress reduction is another appealing factor of automated driving because the average time that the driver of commercial vehicles is behind the wheel is significant; and (c) the ratio of the cost of automation to the cost of vehicle is rather small for commercial vehicles. Since 1993, researchers of the California PATH (Partners for Advanced Transit and Highways) program have conducted a study on lateral control of heavy duty vehicles for automated highway systems (AHS). The group has developed dynamic models of multi-unit heavy vehicles, conducted detailed dynamic analysis of tractor-semitrailer combinations, and designed linear and nonlinear robust control algorithms for lateral control with the magnet-based road reference system. This report is concerned with the most recent effort in this study: i.e. the experimental validation of the linear model for tractor-semitrailer combinations and the implementation of linear robust controller. After sustained effort spanning more than a year, we were successful in getting a vehicle suitable for testing the model and controller designs for automated lane following. A class eight truck was acquired on loan from the Freightliner Corporation of Portland, OR. The truck arrived in the Richmond Field station (RFS) of UC Berkley in October 1997. To complete the test vehicle, a 45 feet long trailer was purchased. In about a year since then, we have developed/installed all the sensors and actuators necessary for demonstrating automated lateral control. The steering actuator, the most important actuator for lateral control was developed by NSK Corporation, Japan, based on PATH's specifications. Brake and throttle actuators for longitudinal control and for differential braking were installed. The sensors needed for lateral control were mounted using in-house fabrication facilities. In the month of October 1998, in about a year after the tractor was acquired, all the instrumentation was installed, tested and calibrated. The first open loop tests to validate the control model were conducted in September 1998 at the Crow’s Landing test site. The experimental vehicle was excited by sinusoidal steering inputs and the outputs of on-board sensors were recorded; the error sensor output was synthesized based on the recorded data; and the frequency response at the excitation frequency was determined. Based on this data, the linear model was calibrated. The calibrated dynamic model of the vehicle was augmented by the steering dynamics, which was calibrated by a separate study. Two linear robust controllers were designed: one based on direct loop shaping of the overall open loop dynamics and the other based on the H-infinity robust control theory. In November 1998, the first closed loop tests were conducted on the tractor-semitrailer vehicle. The results of the experiments are encouraging. Linear controllers achieved a good performance for speeds up to 45 mph on curves and for curve transitions equivalent to 400 m in radius. On straight roads, the controllers were tested to be effective for speeds up to 60 mph.

While linear controllers performed well under normal conditions of pavement and for nominal vehicle parameters, robust controllers are desirable for ensuring stability under perturbed environment and vehicle parameters. With this objective, a robust Sliding Mode Controller is designed. The design is verified in simulations and is shown to be robust to parametric changes of the simulation model.

This report presents the experimental setup, control design and closed loop experiments. The report is organized as follows. Section 2 describes the experimental set up of the vehicle. We will describe the actuators and sensors that have been installed. The development of steering actuator will be discussed. Section 3 presents brief description of the linear model of tractor semitrailer and its properties. Lateral position response to road wheel angle synthesized from open loop data is presented. Section 4 presents the design of a classical linear loop shaping controller, an $H_\infty$ linear loop shaping controller and an SMC.. Section 5 presents closed loop results of implementing the linear controllers on tractor semitrailer vehicle. Conclusions and future work are presented in Section 6.

## 2 Experimental Vehicle

Within the PATH program, the year 1997-1998 has been a landmark year for experimentation of heavy vehicles. Freightliner provided us with a class eight truck, FLD-120. We also acquired a 45' trailer, Great Dane, to complete the experimental vehicle (See Fig. 1). The tractor has a Detroit Diesel engine and Allison World Transmission. It has dual axles in the rear, one of which is the drive axle. There is a fifth wheel on the tractor to hitch the trailer. The Steering system incorporates re-circulating ball type hydraulic assist mechanism.

Fig. 1 Freightliner Tractor and Semitrailer

The installation of sensors and actuators was initiated in December 1997. The test vehicle has now been installed with sensors and actuators for both lateral and longitudinal control. The sensors installed on the vehicle are:

(1) Magnetometers for measuring distance from lane centerline
(2) Gyroscopes and accelerometer for inertial measurements
(3) Steering and road wheel angle sensors
(4) Articulation angle sensor

The actuators installed are:

(1) Steering actuator
(2) Brake actuator

The test vehicle has throttle by wire which is used for actuating fuel command to the fuel injectors. Fig. 2 shows the location of the sensors and steering actuator on the vehicle.

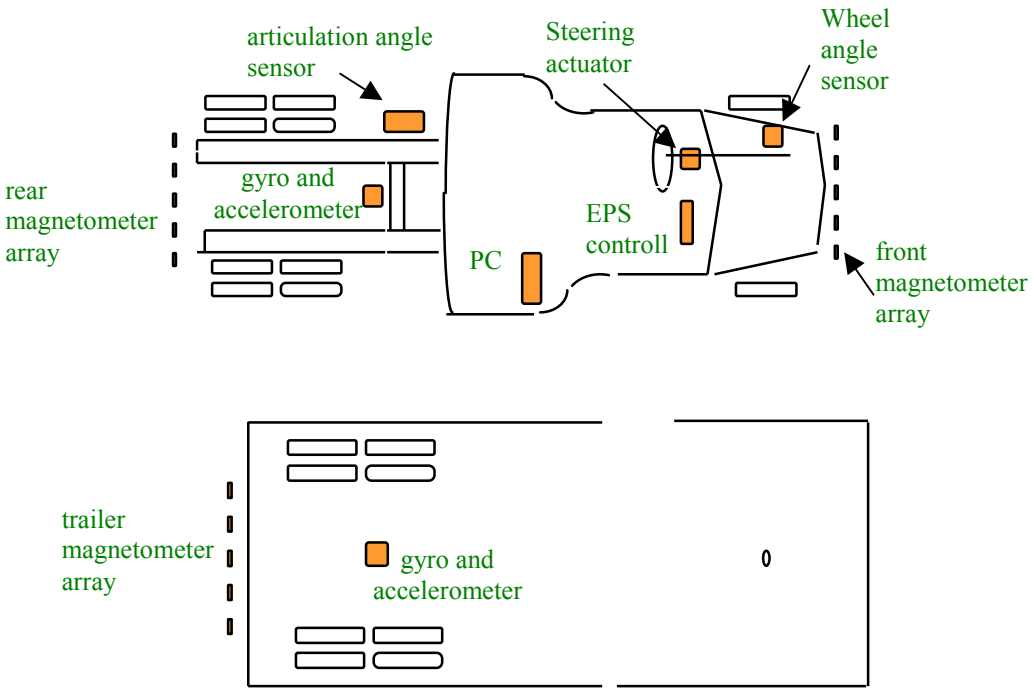


Fig. 2 Sensors and Actuator for Vehicle Lateral Control

## 2.1 Steering Actuator

For the purpose of automatic lateral control, an actuator to track the road wheel angle to a desired value is needed. One of the approaches to developing a steering system is to

redesign the steering system of the truck to accommodate an actuator for automated steering applications. This approach involves redesigning the steering system of the vehicle. Instead of this approach, it was decided to append the pre-existing steering system of the test vehicle with a steering actuator. Design of servo control for such a steering actuator depends on the steering system itself. Therefore, a brief description of the pre-existing steering system on the truck is presented. The schematic of the steering system is shown in Fig. 3.

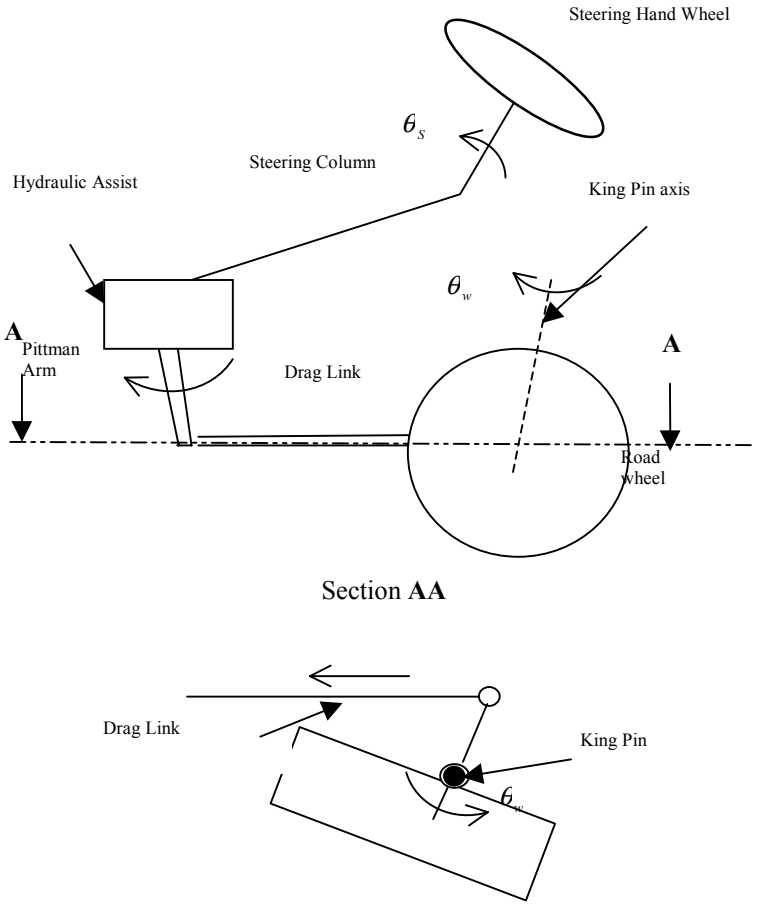


Fig. 3 Steering system of Freightliner Truck

Fig. 4 Steering actuator mounted on the steering column

**2.1.1 Pre-existing steering system**:
Steering system in the Freightliner truck is comprised of many components (see Fig. 3). These include the steering wheel and column, the power assistance unit, the steering linkages connecting the hydraulic power steering unit to the front wheel assembly. The front wheel assembly includes pittman arm, drag links and the wheels. The turning of the steering wheel by angle $\theta_s$ (see Fig. 3) results in the road wheel angle turning by angle $\theta_w$. The hydraulic assist mechanism provides a torque amplification and assists the driver in steering the vehicle.

**2.1.2 Steering actuator**
Figure 4 shows the picture of the steering system with actuator mounted on the steering column. The actuator was mounted on the steering column in order to take advantage of the torque boost provided by the hydraulic assist mechanism. The steering actuator system consists of a D.C. motor with a clutch and an Electrical Control Unit (ECU). ECU is a current controller and at matching loads, provides current proportional to a command voltage. ECU also controls the clutch. The clutch can be turned on and off by giving a digital command to the ECU. The clutch forms an active component of the safety system.

Next subsection gives a dynamical description of the steering system with the actuator.

## 2.3 Steering system model

In this subsection, a mathematical model is developed to look into the dynamical characteristics of the steering system. Previous studies on hydraulic steering systems have shown the existence of position dependent friction, dead zone and nonlinear power boost curve, whose gain characteristics are speed dependent. Also, there is an aligning torque exerted on the front wheels which is a result of the road-wheel interaction and the geometric characteristics of the road wheel assembly such as the caster angle. Modeling all of these effects is not trivial and may not give a model transparent enough for the controller design. Therefore, it is attempted to model the steering system as a two mass system. The D.C motor, the steering wheel and the steering column are lumped as a rigid mass. The front wheel assembly is also lumped together. This model is shown in Fig. 5a

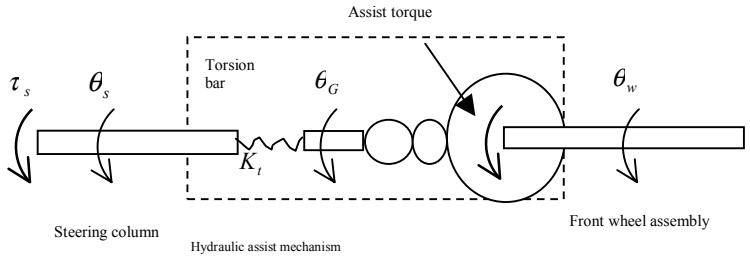


Figure 5a Steering system model

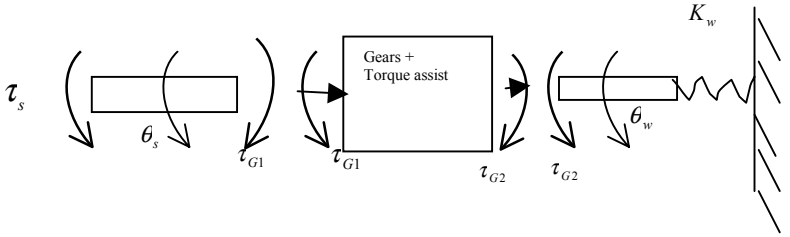


Figure 5b Free body diagram of system in 5a

and 5b. Preliminary experiments have indicated that the dynamic friction and damping coefficients in the motor and the steering column are at least one order smaller than those of hydraulic unit and kingpin. The steering actuator has a rising time of 10*ms,* which is negligible compared to the rising time of the whole steering system (1.5*s*). Since the actuator is mounted towards the hand wheel, the compliance between the hand wheel and the steering column is small. The steering system has in-series stiffness: the stiffness of the steering column, the torsion bar, and the front wheel linkage. The torsion bar is a component of the hydraulic power assistance unit, and it connects the steering column to the ball screw of the hydraulic unit. It serves as a torque sensor for regulation of the hydraulic flow of the power assistance unit. From the above analysis, the steering system is modeled as a two mass system: the steering hand wheel and the steering column are lumped as a rigid body, and the front wheel assembly, pitman arm and drag links are lumped together as another rigid body. The lumped masses are joined by the torsion bar of the hydraulic power assistance unit.

The input to the steering system is a voltage command to the ECU. ECU regulates the current in the DC motor to a value proportional to the command. Assuming that the motor constant is a fixed number, the command is thus the reference for motor torque $\tau_s$. For this reason, the voltage command to the ECU will be referred to as the torque command. Figure 5a represents the model of the steering system with $\tau_s$ as the input to the steering column. The rotation of the steering column is denoted by $\theta_s$. The steering column is connected to the hydraulic assist unit by a torsion bar (see Fig. 5a). The torque in the torsion bar is denoted by $\tau_{G1}$ and is the input torque to the re-circulating ball hydraulic assist unit. The amplified torque is denoted by $\tau_{G2}$, and the road wheel angle by $\theta_w$. Writing torque balance equations for the steering column and the front wheel assembly, we obtain

$$I_s\ddot{\theta}_s + D_s\dot{\theta}_s + \tau_{G1} = \tau_s \tag{1}$$

$$I_w\ddot{\theta}_w + D_w\dot{\theta}_w + K_w\theta_w = \tau_{G2} \tag{2}$$

where $I_s$ and $I_w$ are the lumped inertia of the steering column and the front wheel assembly respectively. $D_S$ is the viscous damping of the steering column, $D_W$ is viscous damping associated with the front wheel assembly and $K_w\theta_w$ is the aligning torque. The torque in the torsion bar, $\tau_{G1}$, is given by

$$\tau_{G1} = K_t(\theta_s - \theta_G) \tag{3}$$

where $(\theta_s - \theta_G)$ is the angular twist in the torsion bar and $K_t$ is the torsional spring constant. We assume the following kinematic relation for the hydraulic assist mechanism:

$$\theta_G = \eta\theta_w \tag{4}$$

where $\eta$ is the gear ratio between output and input shafts of the hydraulic assist unit. We also assume that the output torque $\tau_{G2}$ of the hydraulic assist unit is related to the input torque $\tau_{G1}$ by:

$$\tau_{G2} = \eta\tau_{G1} + \psi(\tau_{G1}) \tag{5}$$

$\tau_{G2}$ in Eq. (5) is composed of two parts. The first term in RHS of Eq. (5) is torque amplification because of the gear ratio $\eta$ whereas the second term, $\psi(\tau_{G1})$, is the hydraulic torque amplification. The function $\psi(.)$ is the characteristic torque assist curve also known as the boost curve. The typical shape of the boost curve is given in Fig. 6 (Automotive Handbook, 1993). Equations (1)-(5) describe the steering dynamics. Note that Eq. (5) makes the model nonlinear.

To facilitate linear analysis, we approximate the boost curve by

$$\psi(x) = \psi_0 x \tag{6}$$

This approximation is shown by the dotted line in Fig. 6 and denotes the "average" over an operating range of input torque $\tau_{G1}$. The validity of approximation in Eq. (6) is moot and further investigation is needed .

Taking Laplace transformation of Eqs. (1) and (2) and using Eqs. (3) to (6), we obtain

$$[s^2 I_w + sD_w + (K_w + R' K_t \eta)]\Theta_w(s) = R' K_t \Theta_s(s) \tag{7}$$

and

$$[s^2 I_s + sD_s + K_t]\Theta_s(s) = \mathrm{T}_s(s) + K_t \eta \Theta_w(s) \tag{8}$$

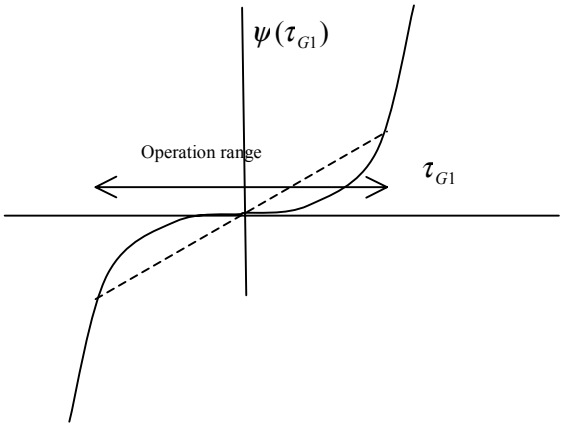


Fig. 6 Boost curve for re-circulating ball type hydraulic assist

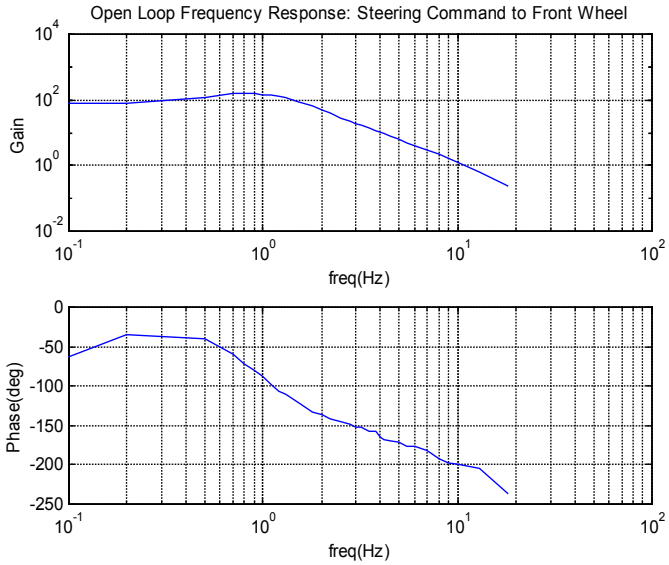


Fig. 7 Open loop frequency response from torque command to front wheel angle

where $R' = \psi_0 + \eta$, $\Theta_s(s)$ is the Laplace transform of $\theta_s$ and $\Theta_w(s)$ denotes Laplace transform of $\theta_w$. Eliminating $\Theta_w(s)$ from (7) and (8) we obtain

$$\Theta_s(s) = \frac{s^2 I_w + sD_w + (K_w + R' K_t \eta)}{D(s)} \mathrm{T}_s(s) \tag{9}$$

where $D(s) = s^4 I_w I_s + s^3 (I_w D_s + I_s D_w) + s^2 [I_w K_t + I_s (K_w + R' K_t \eta) + D_s D_w] + s[K_t D_w + (K_w + R' K_t \eta) D_s] + K_w K_t$

and $\mathrm{T}_s(s)$ is the Laplace transform of $\tau_s$. Using Eq. (7) and substituting for $\Theta_s(s)$ in Eq. (9), we obtain

$$\Theta_w(s) = \frac{R' K_t}{D(s)} \mathrm{T}_s(s) \tag{10}$$

From the perspective of vehicle lateral control, the wheel angel $\theta_w$ must be controlled to a desired value. Transfer function from the torque command to the road wheel angle given by Eq. (10) has a relative degree of four. This is higher than the relative degree of the steering column response by two (see Eq. (9)). Therefore, controlling the road wheel position by torque command is more difficult than controlling the steering column position. Furthermore, the noise in measurement of the wheel angle (electrical as well as mechanical) adds constraints to the controller design. The relative simplicity of Eq (9) over Eq. (10) and virtually noise free measurement of the steering column angle makes the feedback control of steering column angle a more practical approach. It will be shown later that this approach works well because the road wheel follows the steering column without significant lag over the frequency range of interest.

### 2.1.4 Open loop experiments

Some parameters that appear in Eq. (9) may be determined by component wise study (e.g. $I_w$ and $I_s$), and others are difficult to obtain. Consequently, we have not yet succeeded in fully utilizing the nonlinear model given by Eqs. (1)-(5). Equation (9) quantifies the linear dynamical relation between the steering column position to the torque command given to the ECU. In order to verify the structure of the model, open loop experiments were carried out on the steering system. Figure 7 shows a typical response of the steering wheel angle to the torque command. The vehicle was stationary during the experiments. The front wheels were kept on lubricated steel plates to eliminate the effect of friction between road and tires.

To preserve the linearity assumptions of the model, a low amplitude torque excitation was given to the steering actuator. From Fig. 7, it can be seen that at frequencies less than 1 Hz, the magnitude of the response is flat. This is an expected behavior. At low frequencies, the constant terms in the numerator and denominator of Eq. (9) dominate. Therefore the magnitude of transfer function (9) evaluated at low frequencies is flat. On the other hand, the phase plot of the experimental frequency response deviates from the model (9) at low frequencies. Equation (9) predicts the phase shift to be asymptotic to zero at low frequencies. The difference in the actual phase characteristics and that of the model is attributed to nonlinear friction forces from various parts of the steering system which have not been taken into consideration. At frequencies from 2 to 10 Hz, the system behaves like a second order system. This corroborates the relative degree 2 of the model in Eq. (9). The deviation from second order dynamics at high frequencies (greater than 5 Hz) is attributed mostly to the delays and flexure in the actuator drive. The bandwidth of the vehicle dynamics is about 0.3 Hz (Hingwe et al., 1999). On the other hand, the bandwidth of the steering system is about 1 Hz (see Fig. 7). Based on this, it may be concluded that a steering system model characterizing the response up to 5 Hz may be sufficient for the controller design. One such model is given by

$$\Theta_s(s) = \frac{166}{[s^2 + 2\pi s + 4\pi^2]/4\pi^2} V(s) \tag{11}$$

where $V(s)$ is the Laplace transform of the torque command to the ECU. This model deviated from the real system only at frequencies higher than 5 Hz and at frequencies lower than 0.2 Hz. The design of the steering controller presented in the next section assumes the model described by Eq. (11).

### 2.1.5 Loop shaping controller design

The structure of the local control loop is shown in Fig. 8. The difference between the reference steering wheel angle and the actual steering wheel angle is the input to the position controller (inner loop controller). The output of the controller is the torque command to the ECU. To regulate the steering wheel position error to zero, a loop shaping controller is designed.

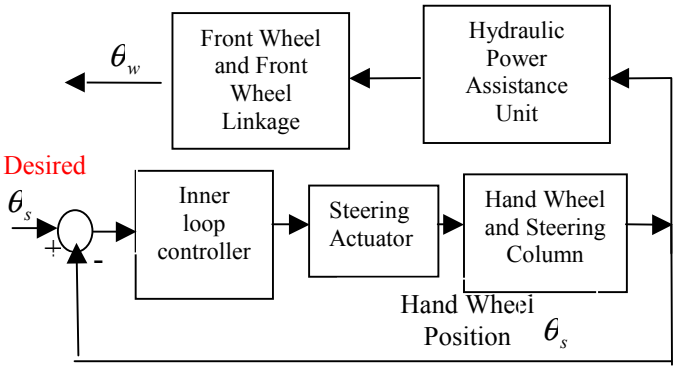


Fig. 8 Closed loop block diagram of the steering subsystem

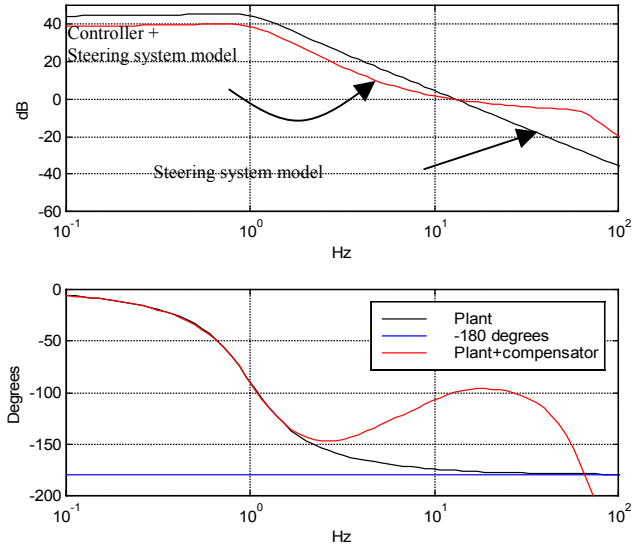


Fig. 9 Second Order Linear Model of the Steering System and Loop Shaping Controller

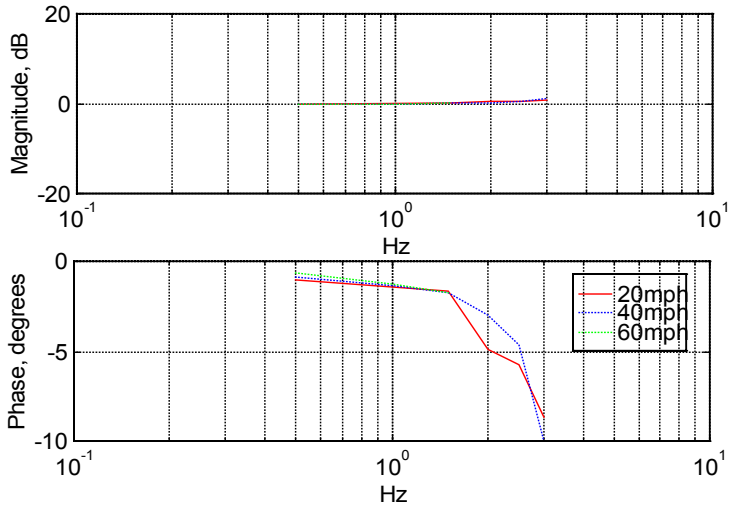


Fig. 10 Closed loop response of the steering actuator

To compensate nonlinear friction forces at low velocities, high gain control is desired at low frequencies. High gain control over all frequencies will reduce the stability margin or even destabilize the closed loop system (see Fig. 7). Therefore the design choice is: (a) use a proportional controller with low gain to retain stability of closed loop or (b) use a controller with high gain at low frequencies and add phase lead selectively at the target gain cross over frequency. A proportional controller was tested experimentally. The gain could not be made high enough to make the steady state error acceptable. Therefore, the second option was adopted as the design choice. Phase lead at a target crossover frequency was introduced by a lag lead compensator. To filter high frequency noise and avoid excitation of high frequency dynamics, a roll off filter was also added. Design iterations were conducted so as to make the low frequency gain of the compensator sufficiently high. The transfer function of the controller selected for closed loop testing is given by

$$0.43\,\frac{7.88\,(s+33)}{(s+260)}\,\frac{640\,(s+250)}{(s^2+400\,s+160000)}\,F(s) \tag{12}$$

$F(s)$ is given by

$$F(s)=\frac{(s^2+1.4\omega_1 s+\omega_1^{\,2})}{(s^2+2\omega_1 s+\omega_1^{\,2})}\,\frac{(s^2+1.4\omega_2 s+\omega_2^{\,2})}{(s^2+2\omega_2 s+\omega_2^{\,2})} \tag{13}$$

where $\omega_1 = 20\pi$ and $\omega_2 = 8\pi$ .

In Eq. (12), $\frac{7.88\,(s+33)}{(s+260)}$ adds the maximum phase lead of about 50 at 15 Hz. The roll off filter is given by $\frac{640\,(s+250)}{(s^2+400\,s+160000)}$. $F(s)$ was added to fine tune the design.

Open loop response of the steering system with and without the compensator is shown in Fig. 9. The steering system illustrated in Fig. 9 is a linear second order model given by Eq. (11). The actual system (Fig. 7) exhibits additional phase lag (with respect to the

second order approximation) at frequencies greater than 5 *Hz*. Therefore, the open loop phase characteristics of the compensated actual steering system is almost a constant -150 degrees from 2 *Hz* till 10 *Hz* after which it drops sharply. The phase margin remains thus about 30 degrees for varying gain crossover frequencies from 2 to 12 *Hz*. The near constant open loop phase provides robustness to gain changes in the system.

### 2.1.6 Closed loop experiments

The controller presented in Section 2.1.5 was implemented digitally. The sampling time was 2 ms, and the continuous time controller was transformed to a digital controller by the bilinear transformation with frequency pre-warping at 10 Hz. The closed loop experiments were carried out at 20mph, 40mph and 60mph at the Crow's Landing test site. The result of these tests is shown in Fig. 10.

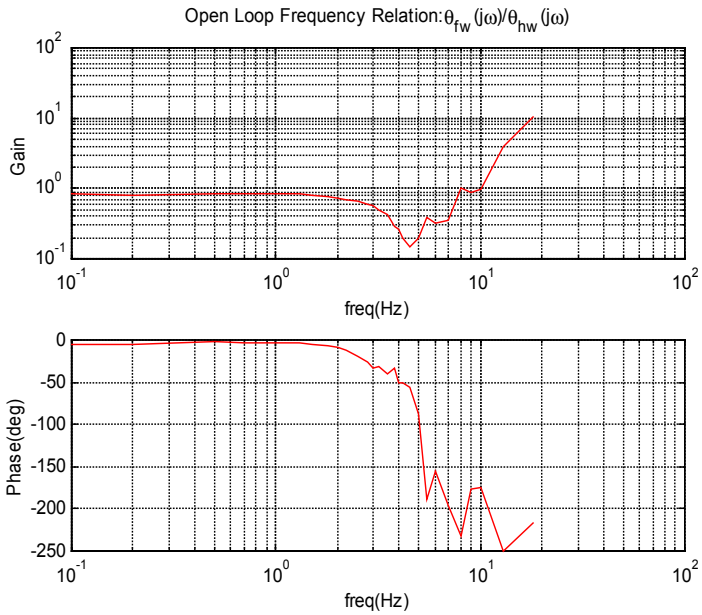


Fig. 11 Response of road wheel to the steering hand wheel

The input to the system was the steering wheel angle command. The output was the actual steering column angle. It can be seen that up to about 1.6 Hz, the closed loop controller is quite effective. At 3 Hz, however, there is a phase delay of about 10 degrees. On the other hand, the magnitude of the actual steering wheel response to the desired steering angle is nearly unity. This indicates a nonlinear behavior or a possible delay.

The steering actuator controller is effective in tracking the desired steering column angle. However, from the vehicle lateral control perspective, the goal is to control the road wheel angle to a desired value. Figure 11 relates the hand wheel and the front wheel in the frequency domain. It can be seen that the front wheels follow the steering column without significant delay up to about 2 Hz. The vehicle bandwidth is about 1 Hz. Therefore, controlling the steering wheel instead of the road wheel angle is justified.

## 2.2 Brake Actuator

Originally, the tractor semi-trailer had an air brake system. In this system, the air from the

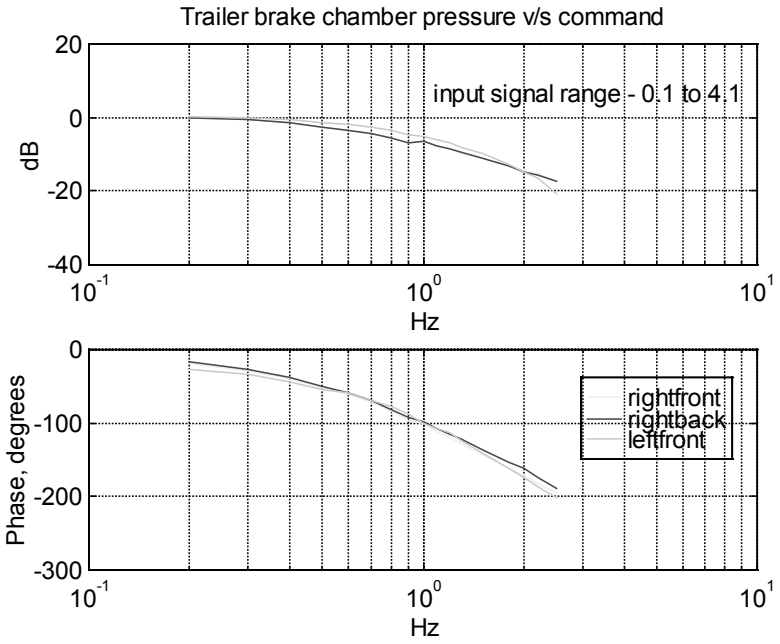


Figure 12. Frequency response of the brake subsystem
(input: command to proportional valve, output: chamber pressure)

storage tanks is delivered to the brake chambers proportional to the pressure in the "service line". Pressure to the service line is controlled by the foot pedal operated by the driver. Over this system, a parallel electronic control system was installed. The electronic system controls the pressure in the brake chamber. The brake chamber diaphragm is connected to an "S" cam by linkages such that increase of pressure in brake chamber pushes the brake shoes against the brake drum via the "S" cam and other linkages. The tractor has six brake chambers (two per axle) and the trailer has four brake chambers (two per axle). Each brake chamber is fitted with a pressure sensor. There is a proportional air pressure controller for the brake chambers on the front axle of the tractor. Another proportional controller controls pressure to the rear axle chambers of the tractor. Trailer has differential braking capability. This is achieved by controlling the pressure to the right brake chambers of the trailer axe independent of the left brake chamber pressure. The differential braking capacity will be utilized in future for enhanced lateral control. The schematic of the pressure transducers and actuators is shown in Fig. 13. The main components of the electronic brake control system are electronic proportional valves. The proportional valves translates voltage command to a proportional pressure in the pressure chambers. The dynamic response of the pressure in the brake chamber to the pressure command signal was measured and is given in Fig. 12.

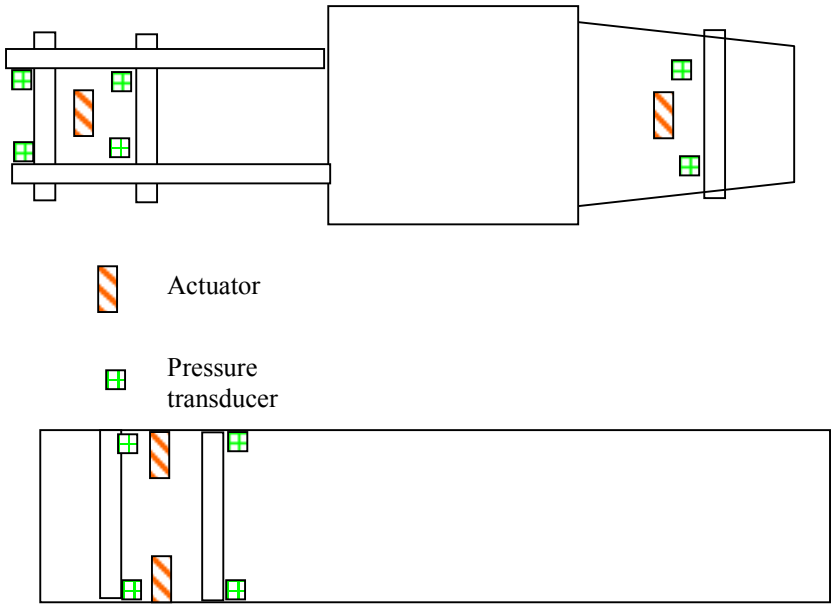


Figure 13. Schematic showing locations of the brake pressure sensors and the actuators on the vehicle

Fig. 14 Brake Actuator

Fig. 15 Air Pressure Transducer

## 2.3 Sensors on the test vehicle

### 2.3.1 Lateral error sensors

In vehicle lateral control for AHS, it is critically important how the vehicle's position and orientation relative to the road are obtained. Various road reference/sensing systems have been proposed in the past. Perhaps, the oldest among them are wire reference systems (Fenton, et al., 1976; Gardels, 1960). Other schemes include an optical marker system, an optical line following system, various radar- and vision-based systems, a side-looking radar system with a reference wall, GPS systems, and magnetic marker (nail) system with on-board magnetormeters. Guidance by permanently magnetized markers was studied in the early 1970's (Mahrt, 1992). This scheme was revived in the late 1980's by PATH (Zhang, et al., 1990). PATH researchers developed robust signal processing schemes for obtaining the lateral error, as well as, encoding schemes to embed other information such as preview road curvature information in binary form by alternating the polarity of the magnets. Furthermore, it compares favorably with other schemes in terms of evaluation criteria such as accuracy, reliability, maintainability, and cost. Therefore, the scheme was adopted as the primary reference system in PATH at the early stage, and it has remained as a key element in PATH-AHS.

Fig. 16 Magnetometer Sensor Array

For PATH research on passenger vehicles, an array of three magnetometer, one in the front and the other in the rear of the vehicle was used. The magnetometer in the array were placed 30 cm apart. The array gave a range of 50 cm on either side of the road centerline. For vehicles with long wheel bases, the amount of off-tracking is severe. It has been shown that (depending on speed and the radius of curvature), the amount of off-tracking can be as much as 20 cm. Moreover, slow response of the heavy vehicles means a possibly high transient error at curve transitions. These considerations demand an increased lateral sensing range over passenger vehicles. Therefore, arrays of five magnetometers (See Fig. 16 ) have been installed at each of the front end of the truck, the rear end of the truck and the rear end of the trailer. They have a sensing range of 0.8 m on either side of the lane centerline. Under this project, a new processing algorithm was

designed to increase reliability over the older PATH scheme of lateral error measurement. This scheme has been adopted by other projects in PATH as well. The current scheme, based on look up tables of magnetic field due to magnetic markers, provides accuracy of 1-2cm.

Other sensors which are installed on the test vehicle are given in the following subsections.

**2.3.2 Accelerometers and gyroscopes**, one each on the tractor and semitrailer

The accelerometers mounted are three axis accelerometers. The accelerometers were mounted on a location least susceptible to mechanical vibrations and were rigidly attached to the chassis of the tractor. Unlike the body of passenger cars, the truck chassis provides acceleration measurement which is free of cabin acceleration. In passenger cars, the cabin (body) is part of the chassis. Therefore the chassis acceleration is coupled with cabin acceleration. In addition to the accelerometers, two Gyroscopes, one each on the tractor and semitrailer were also mounted . The accelerometers and gyroscopes shared a common mounting platform. Figure 17 shows a picture of the accelerometer/gyroscope mount.

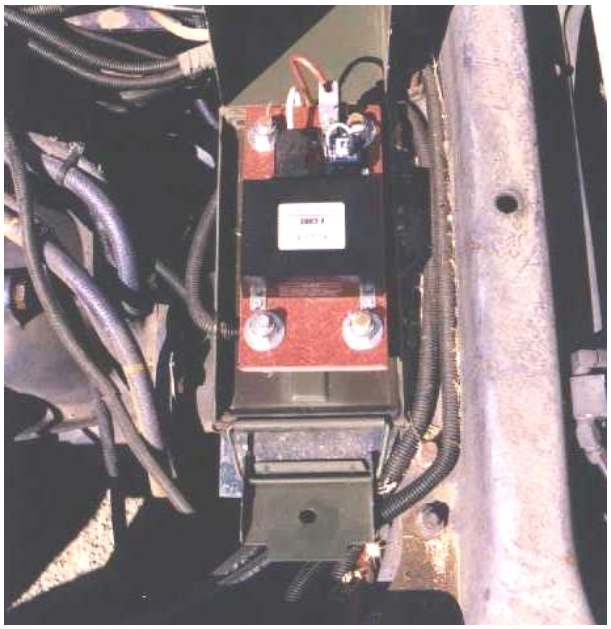

Figure 17 Picture of the accelerometer and gyroscope

**2.3.3 Wheel angle sensor**

A string pot was placed on the hydraulic assist mechanism with its string passing over a sector concentric with the output shaft of the hydraulic assist mechanism. Thus in reality this arrangement measures the pittman arm angle. A true road wheel angle is defined by measuring the rotation around the king pin axis. Nevertheless, the amount of play in the drag link and the king pin is assumed small enough to justify the simpler mounting

solution that we have adopted. The sensor covers the entire range of road wheel angle and gives an accuracy of about half a degree. Figure 18 shows a picture of the road wheel angle.

Figure 18 Picture of the wheel angle sensor

### 2.3.4 Articulation angle sensor

A string pot identical to the one used for road wheel angle was used for the measuring the articulation angle. The string pot was mounted on the truck chassis with its string passing over a sector of radius 25 inch concentric with trailer king pin. The arrangement provides about 60 degrees of articulation angle range on each side with accuracy of less than one degree. Figure 19 gives the schematic for the articulation angle sensor (top view).

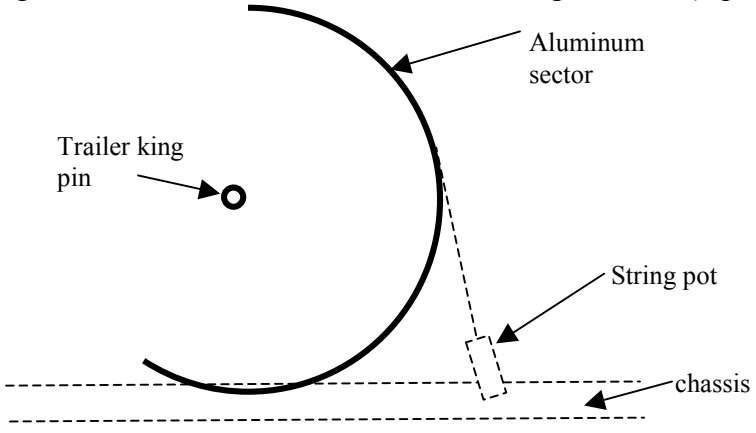


Figure 19 Schematic of the articulation angle sensor

### 2.4 Interfacing and control computer

The sensors are all analog sensors and they interface with a Pentium P.C. through National Instruments DAQ board ATMIO64. The analog inputs are sampled every two

milliseconds. The actuators receive analog signals (commands) from the P.C. through the D/A board (ATMIO 64 being one of them). The software for real time implementation of controllers is based on the previous PATH architecture which was suitably modified to accommodate new sensors and actuators. A signal conditioning board was developed to serve as the interface board between the sensors/actuators and the data acquisition/D-A boards. The board has anti-aliasing filters for filtering noise in analog input channels (for most of the sensor signals), digital input/output channels (for two state devices like clutch etc.), divide by 10 timer interface circuits (for measuring vehicle velocity) and analog output channels (for actuators).

## 3 Tractor semi-trailer model and experimental validation

### 3.1 Dynamic Model

Dynamic modeling of the tractor semitrailer vehicle and of multi-unit heavy vehicles can be found in Chen and Tomizuka,1995a and Tai and Tomizuka, 1998. In this report, we state the linear model and discuss the effect of "look ahead" on control design. California PATH has adopted a magnetic marker based road reference scheme. The road centerline is defined by a series magnets embedded in the pavement along the road centerline and separated by about one meter distance. The vehicle is assumed to have an array of magnetometers. The distance of the magnetometer array (and therefore, of the vehicle) from the magnets is given by the output of a signal processing algorithm. Experiments on lateral control in PATH started with an array of magnetometers at the front bumper of the vehicles. This scheme results in a "look down" sensing of the road reference. It has been shown that a look down scheme imposes severe restriction on the performance of the lateral control scheme (Guldner at al., 1997). Therefore a second array, at the rear end of the vehicles, was proposed. The "lateral errors" at the two independent arrays can then be extrapolated to obtain "virtual error" at a point ahead of the vehicle. It has been shown that feedback of the "virtual lateral error" (with look ahead) makes the lateral controller design easier.

#### 3.1.1 Tractor-Semitrailer Model

The linear lateral dynamics model of tractor-semitrailer is given by.

$$M\ddot{q} + D\dot{q} + Kq = F\delta + E_1\dot{\varepsilon}_d + E_2\ddot{\varepsilon}_d \tag{13}$$

where

$$q = \begin{bmatrix} y_r & \varepsilon_r & \varepsilon_f \end{bmatrix}^T \tag{14}$$

$M, D, K, F, E_1$ and $E_2$ in Eq. (13) are explained in Appendix A. In Eq. (14), the generalized coordinate, $y_r$ is the lateral displacement of the tractor's center of gravity (CG), $\varepsilon_r$ is the tractor's yaw error relative to the road orientation and $\varepsilon_f$ is the trailer articulation angle. The input to the system (11) is the steering wheel angle, $\delta$. In Eq. (13), $\dot{\varepsilon}_d$ and $\ddot{\varepsilon}_d$ are the desired tractor yaw rate and the rate of change of yaw rate respectively. $\dot{\varepsilon}_d$ is related to the vehicle speed $v$ and road curvature $\rho$ by $\dot{\varepsilon}_d = \rho v$. Usually, they are treated as disturbances to the system.

By defining the 6×1 state vector as

$$x = \begin{bmatrix} q \\ \dot{q} \end{bmatrix} \tag{15}$$

the linear state-space model is obtained as

$$\begin{aligned} \frac{d}{dt}x &= \begin{bmatrix} 0 & I \\ -M^{-1}K & -M^{-1}D \end{bmatrix} x + \begin{bmatrix} 0 \\ M^{-1}F \end{bmatrix} \delta \\ &+ \begin{bmatrix} 0 \\ M^{-1}E_1 \end{bmatrix} \dot{\varepsilon}_d + \begin{bmatrix} 0 \\ M^{-1}E_2 \end{bmatrix} \end{aligned} \tag{16}$$

It is noted that the system matrices appearing in Eqs (13) and (16) depend on the vehicle speed, tire cornering stiffness and loading of trailer.

The lateral error measurement from the magnetometer arrays is used to generate a "virtual lateral error" at a point ahead of the vehicle body. This lateral error is given by

$$y_s = y_r + d_s \varepsilon_r \tag{17}$$

where $y_s$ is the lateral error at $d_s$ distance ahead of the tractor's CG. This lateral error is synthesized from the output of two magnetometer arrays, one at the front end of the tractor and other at the rear end of the tractor. Therefore, an extrapolation of the lateral error at a distance physically ahead of the vehicle is possible, giving rise to the concept of "look-ahead". The effect of look ahead is illustrated in Fig. 20 by the frequency response of the lateral acceleration to the steering angle as a function of velocity and as a function of look ahead distance $d_s$.

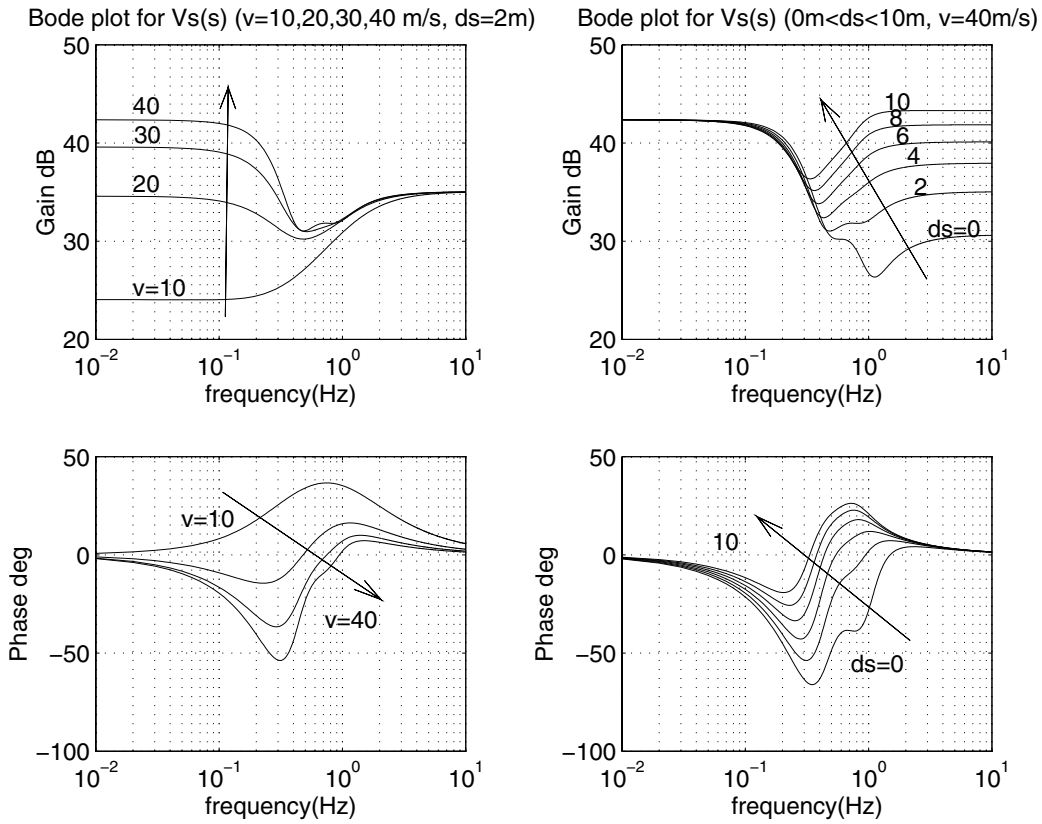


Figure 20 Effect of velocity and look ahead on frequency response of the lateral acceleration at CG to the road wheel angle

Figure 20 shows that the lateral control is a difficult problem at high velocities if lateral error at the CG is measured for feedback. This is because at higher velocities, the phase of acceleration response to the steering is negative at critical frequencies (the bottom left plot in Fig. 20). Therefore the phase shift between the steering input and the position output exceeds –180 degrees at those frequencies. However, if the look ahead distance, $d_s$, is increased, then there is a significant phase gain in the acceleration response (see the bottom right plot in Fig. 20). For further details, reader is referred to Wang and Tomizuka (1998). The controllers that will be described in the following section will use the advantage of the look ahead scheme.

### 3.2 Open Loop Experiments and System Parameter Identification:

The first set of experiments conducted in September 1998 on the tractor-semitrailer were open loop experiments to verify the dynamic model. Sinusoidal reference command (see Fig. 9) was given to the steering actuator. The lateral acceleration of the tractor, the yaw rate response and the velocity of the tractor were recorded. From Fig. 20 and from linear model it is clear that the response of the vehicle varies depending on the longitudinal speed of the vehicle. Therefore separate frequency response tests were conducted at 20mph, 40mph and 60mph. In previous section, it was shown that the look-ahead

distance had an important impact on the control design for tractor semitrailer vehicles (see Fig. 20). For lateral control at high speeds, the advantage of using a certain look ahead distance is clear. Therefore, model verification for such a look-ahead measurement is a natural step to take. The measurements from the accelerometer, yaw rate sensor and the vehicle speed sensor were combined to synthesize the position response of the vehicle at a point $d_s$ distance ahead of the CG. From kinematics, we know

$$a_s = a_{CG} + d_s \ddot{\varepsilon}_1 \tag{18}$$

where $a_s$ is the lateral acceleration at $d_s$ distance ahead of the C.G, $a_{CG}$ is the lateral acceleration at C.G. and $\ddot{\varepsilon}_1$ is the yaw acceleration of the tractor. If the accelerometer is located $d_m$ distance ahead of the CG, then we can write

$$a_m = a_{CG} + d_m \ddot{\varepsilon}_1 \tag{19}$$

where $a_m$ is the acceleration measured by the accelerometer.
From Eqs. (18) and (19), we get

$$a_s = a_m + (d_s - d_m)\ddot{\varepsilon}_1 \tag{20}$$

Laplace transformation of Eq. (20) is given by

$$s^2 Y_s(s) = A_m(s) + (d_s - d_m)s\dot{\mathrm{E}}_1(s)$$

where $Y_s(s)$ is the Laplace transform of the vehicle position at $d_s$ distance ahead of the CG, $A_m$ is the Laplace transform of the measured acceleration and $\dot{\mathrm{E}}_1(s)$ is the Laplace transform of the tractor's yaw rate measurement. All these quantities are measured values. An extrapolation distance of 7.45m ahead of the front magnetometer array was chosen for plotting the synthesized response. The result of this synthesis is shown in Fig 21. The dots in the figure represent experimental data and the solid lines represent the analytical linear model. The parameters of the linear model were tuned to match the experimental data as close as possible. The model and the data agree with each other qualitatively. Efforts will be made to quantify this match in terms of parameter identification of the linear model. The vehicle deviates from the linear model at higher frequencies, which may be attributed to unmodelled dynamics of the tire-road interaction and the suspension system.

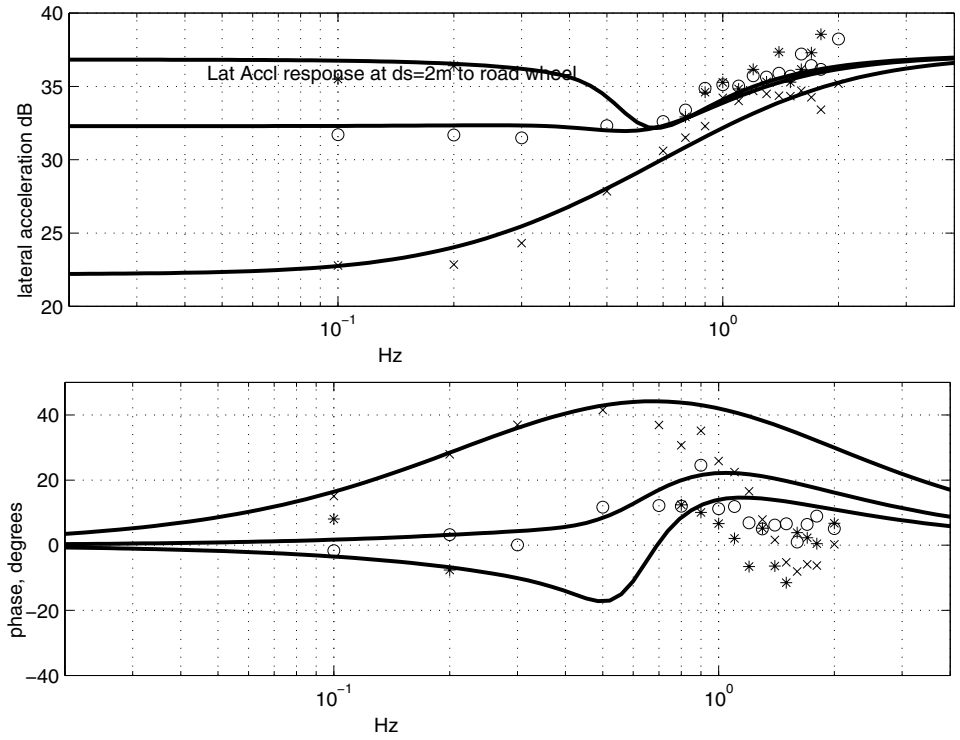


Figure 21 Comparison of the model (solid lines) and the open loop data (dots) for different longitudinal vlocities

## 4 Lateral Controller for Tractor-Semitrailer Vehicle

Controllers based on linear and nonlinear theory have been developed for lateral control of tractor semitrailer combination (Chen and Tomizuka, 1997). FSLQ based controller was designed by Chen and Tomizuka (1996). Nonlinear controllers based on input output linearization has also been designed (Chen and Tomizuka 1996). Moreover, a controller for combined steering and brake control based on back stepping has been designed (Chen and Tomizuka 1995b). For actual implementing and testing of the lateral controller, it was decided to start with linear fixed gain controllers which are the simplest among other alternative controllers. For this purpose, it was decided to implement two linear controllers, one based on classical loop shaping and other based on $H_\infty$ loop shaping. Apart from these, a sliding mode controller for the tractor-semitrailer systems was developed. Next subsections give a description of these controllers.

### 4.1 Classical loop shaping controller

From the linear response of the vehicle, we can see that the vehicle system itself provides adequate phase margin for velocities below 20mph. This means that a proportional controller will stabilize the closed loop system (i.e., will regulate the system around zero tracking error). However, at higher velocities, the phase drops significantly (Fig 20) and proportional controller will not work. Thus, it is necessary to design a compensator which

will provide phase margin sufficiently large for robustness; in particular at high velocities. With this objective, a loop shaped controller design was attempted.
The design criteria were

(i) The look-ahead distance was kept to 7.4 meters. Note that the response plotted in Fig 21 is for this look ahead distance.
(ii) Open loop gain (vehicle and the compensator) should be high at low frequencies (smaller than 0.05 Hz). This will minimize the tracking error at steady state.
(iii) The vehicle has a phase lag of more than 180 degrees at gain cross over frequency (approx. 0.3 Hz), especially at high speeds. Therefore the compensator needs to add appropriate phase lead at this frequency.
(iv) To avoid steering responding to measurement noise, the compensator gain beyond 0.5 Hz should be small

With these criteria in mind, a loop shaping controller was designed. High loop gain at low frequency is assured without an integrator because the plant itself has very high gain at low frequencies (a double integrator behavior). To advance phase at 0.3 Hz , a lead component is added. To offset the high frequency gain by the lead compensator, a roll off filter and a lag filter are added. The lag compensator introduces phase lag at frequencies much lower than the cross over . At these frequencies, the plant has a high gain but phase lags more than –180 degrees. The over all system may still remain stable as explained by the Nyquist plot in Fig. 22. In the Figure, $G(j\omega)$ is the frequency response of vehicle and compensator in series. We see that the controller is conditionally stable in terms of the gain. Therefore, a gain such that the Nyquist plot did not encircle –1 must be selected.

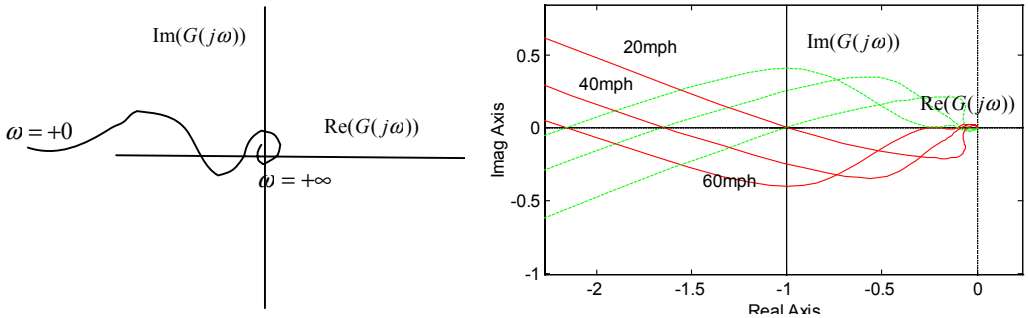


Figure 22 Nyquist plot of the loop tranfer function of closed loop

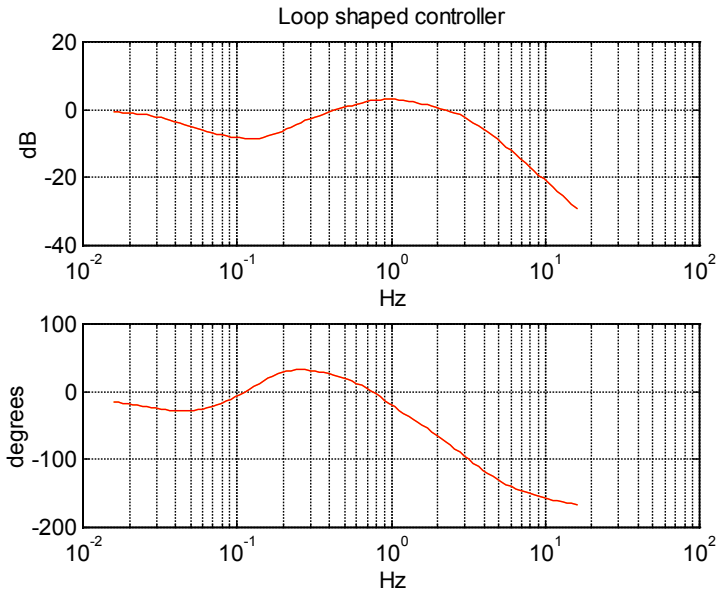


Fig. 23 Loop shaped controller

The transfer function of the controller is given by

$$Gain^{*}\frac{s^{6}+11.69s^{5}+48.97s^{4}+65.66s^{3}+59.99s^{2}+24.76s+6.31}{0.0028s^{8}+0.10s^{7}+1.87s^{6}+13.94s^{5}+62.60s^{4}+118.88s^{3}+104.13s^{2}+41.96s+6.31}$$

The frequency response is shown in Fig 23. The Loop shaped controller has been tested at speeds upto 45 mph on curve transitions of +800m to -800m and up to 60 mph on straight sections.

### 4.2 Robust H-infinity Loop Shaping

This section addresses the robust steering control problem for a single HDV (tractor-semitrailer type) using the H-infinity loop shaping design procedure (LSDP) which was proposed by McFarlane and Glover (1989). It was pointed out that variations of vehicle longitudinal speed and road adhesion coefficient have significant influence on vehicle dynamics (Patwardhan et al ,1997, for passenger cars ; Wang and Tomizuka ,1998, for HDVs). Varying cargo loads is another important cause of uncertainties for HDVs. Robustness against these model uncertainties will be discussed in the H-infinity synthesis. Generally speaking, H-infinity loop shaping is a two stage design procedure. First, the open-loop plant is augmented by pre and post-weighting filters to give a desired shape for the singular values of the open-loop frequency response. The resulting shaped plant is then robustly stabilized with respect to coprime factor uncertainty using H-infinity optimization. Controllers obtained by H-infinity loop shaping have some advantages over other H-infinity-based methods. For instance, no $\gamma$ -iteration is needed for the solution, and explicit formulae for the corresponding controllers are available. In particular, they do not exhibit stable pole-zero cancellation, which is common in many H-infinity control problems and is undesirable if the plant has lightly damped modes (Sefton

and Glover ,1990 , Tsai et al ,1992). This method has been successfully applied to several industrial problems (Hyde ,1991, Postlethwaite and Walker ,1992, and Fujita et al ,1993). Mammar (1996) and O'Brien et al (1996) conducted similar approaches on automated passenger vehicles.

### 4.2.1Control design objectives and constraints

In Eq. (13), *M* is a function of $m_2$ (cargo loads in the trailer) and *D* is a function of *v*, $m_2$ and $\mu$ (road adhesion coefficient, 1 for dry road surface and 0.5 for wet road surface). *F* and *K* are functions of. Variation of these parameters will cause model uncertainties. As described earlier, we define $y_s$ as the lateral displacement of the virtual look-ahead sensor which is placed $d_s$ meters ahead of the tractor CG, i.e.

$$y_s = y_r + d_s \varepsilon_r \tag{21}$$

The lateral error at the virtual sensor is obtained from the extrapolation of two magnetometer readings (they are located at the front axle and the rear axle of the tractor respectively). As shown in Patwardhan et al (1997) and Wang and Tomizuka (1998), by regulating $y_s$ instead of $y_r$ to zero, we can increase the phase lead of the system dynamics and have more strongly damped zeros for the open-loop system. Increasing $d_s$ enlarges phase lead even at high speeds. However there may exist a large lateral offset error at the tractor CG and the sensor noise will be amplified if a large look-ahead distance $d_s$ is chosen. Thus there is a trade-off between the phase margin we can get by redefining the output and the tracking performance we can achieve by regulating $y_s$. In this section, we choose $d_s$=5m for the controller design and implementation.

Considering the average lane width on US highways and the average width of the HDVs, a small lateral tracking error at the tractor's CG is required (less than 0.2 m). Since the trailer is relatively long, a small off-tracking error at the rear of the trailer is also desired. The designed controller should be robust against model uncertainties. We assume that the speed range for HDV is 0 to25 m/s (0 to 56.25 mph) and that the road adhesion coefficient varies from $\mu$ =0.5 to $\mu$ =1. Cargo loas in the trailer varies from $m_2$=5000 kg to $m_2$=24000 kg. The steering action is generated by the steering actuator which has a limited bandwidth. The steering rate is limited to 28 deg/s and steering angle is confined to 30 degree. In simulation, an additional time delay of 15 ms is added to the approximated first-order steering actuator dynamics.

### 4.2.2 Robust Stabilization Problem

First, we give some definitions:

**Definition 4.1**: Left Coprime (LC): Supose $M, N \in RH_\infty$ have the same number of rows. Then *M* and *N* are left coprime if and only if (iff) $\exists U, V \in RH_\infty$ such that *MV-NU=I*

**Definition 4.2:** Left Coprime Factorization (LCF): The pair *(N,M)*, where $M, N \in RH_\infty$, constitutes a left coprime factorization of $G \in R$ iff

(a) $M$ is square and $|M| \neq 0$

(b) $G = M^{-1}N$

(c) *(N,M)* is LC.

**Definition 4.3:** Normalized Left Coprime Factorization (NLCF): The pair *(N,M)*, where $M, N \in RH_\infty$, constitutes a normalized left coprime factorization of $G \in R$ iff *(N,M)* is a LCF of $G$, and in addition $NN^* + MM^* = I$

The next Lemma (Vidyasagar , 1985 ) summarizes the existence and uniqueness properties of a NLCF.

**Lemma 4.1:** The normalized left coprime factors $N$ and $M$ of a transfer function $G \in R$ exist and are unique to within left multiplication by a unitary matrix.

We will consider the stabilization of a plant G which has a normalized left coprime factorization (NLCF) *(N,M)*:

$G = M^{-1}N$

A perturbed plant $G_\Delta$ can be written as

$G_\Delta = (M + \Delta_M)^{-1}(N + \Delta_N)$

where $\Delta_M$ and $\Delta_N$ are stable unknown transfer functions which represent the uncertainty in the nominal plant model $G$. The objectives of robust stabilization is to stabilize not only the nominal plant $G$ but also a family of perturbed systems defined by

$G_\Delta = \{(M + \Delta_M)^{-1}(N + \Delta_N) \ : \Delta = [\Delta_M \Delta_N] \in D_{S_\varepsilon}\}$

where

$D_{S_\varepsilon} = \{\Delta : \Delta \in RH_\infty, \|\Delta\|_\infty < \varepsilon\}$

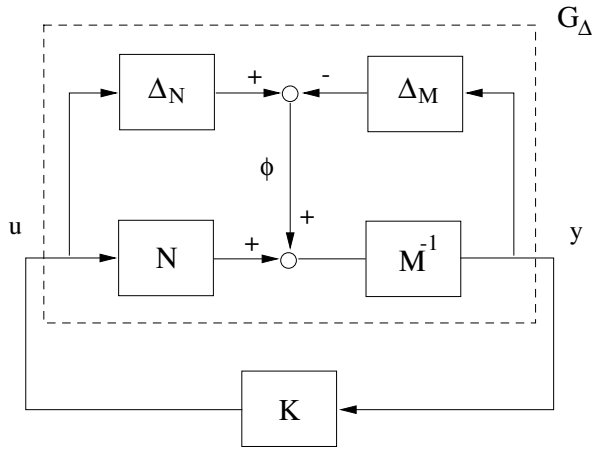


Figure 24 H-infinity robust stabilization problem

The following theorem gives the necessary and sufficient conditions for the stabilizing controller *K*.

**Theorem:** The controller *K* stabilizes $G_\Delta = (M + \Delta_M)^{-1}(N + \Delta_N)$ in Fig. 24 for all $\Delta = [\Delta_M \Delta_N] \in D_{S_\varepsilon}$ iff

(a) *K* stabilizes *G*

(b) $\gamma = \left\| \begin{bmatrix} K \\ I \end{bmatrix} (I - GK)^{-1} M^{-1} \right\|_\infty < \varepsilon^{-1}$

Note that s $\gamma$ is the H-infinity norm from $\phi$ to $[u \quad y]^T$ and $(I - GK)^{-1}$ is the sensitivity function for this positive feedback arrangement shown in Fig. 24. The lowest achievable value of $\gamma$ and the corresponding maximum stability margin $\varepsilon$ are given by McFarlane and K. Glover (1989):

$$\gamma_{\min} = \in^{-1}{}_{\max} = \{1 - \left\|[N.M]\right\|_H{}^2\}^{\{1/2\}} = (1 + \rho(XY))^{\{-1/2\}} \qquad (22)$$

where $\left|...\right|_H$ denotes the Hankel norm and $\rho$ denotes the spectral radius (the maximum eigenvalue). *X* and *Y* are the unique positive definite solutions of the following algebraic Ricatti equations:

$$(A - BS^{-1}D^T C)^T X + X(A - BS^{-1}D^T C) - XBS^{-1}B^T X + C^T R^{-1} C = 0 \qquad (23)$$

$$(A - BS^{-1}D^T C)Y + Y(A - BS^{-1}D^T C)^T - YC^T R^{-1} CY + BS^{-1}B^T = 0 \qquad (24)$$

where $R = I + DD^T, S = I + D^T D$

A ``central'' controller proposed in McFarlane and K. Glover (1989), which guarantees that

$$\left\| \begin{bmatrix} K \\ I \end{bmatrix} (I - GK)^{-1} M^{-1} \right\|_\infty < \gamma$$

for a specified $\gamma > \gamma_{\min}$, is given by

$$A_K = A + BF + \gamma^2 (L^T)^{-1} YC^T (C + DF)$$

$$B_K = \gamma^2 (L^T)^{-1} YC^T$$

$$C_K = B^T X$$

$$D_K = -D^T$$

$$F = -S^{-1}(D^T C + B^T X)$$

$$L = (1 - \gamma^2) I + XY$$

where $(A_K, B_K, C_K, D_K)$ is the state-space realization of the central controller *K*. Since $\gamma_{\min}$ can be computed from Eq. (22), we can get an explicit solution by solving just two Ricatti equations (Eqs. (23) and (24)) thus avoiding the $\gamma$-iteration needed to solve the general H-infinity problem.

### 4.2.3H-infinity Loop Shaping Design Procedure (LSDP)

Robust stabilization alone is not practical because the designer is not able to specify any performance requirements. McFarlane and Glover, (1989) proposed pre- and post-compensation of the plant to shape the open-loop singular values prior to robust stabilization of the ``shaped plant''. First, choose $W_1$ and $W_2$ as the pre- and post-weighting filters respectively; the resulting shaped plant $G_S$ is given by $G_S = W_2 G W_1$ as shown in Fig. 25 (a).

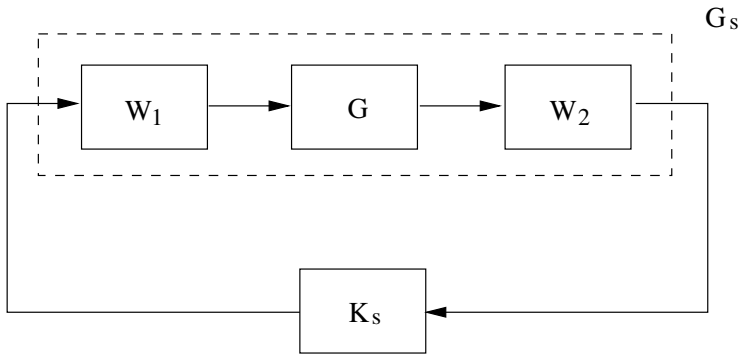


(a)

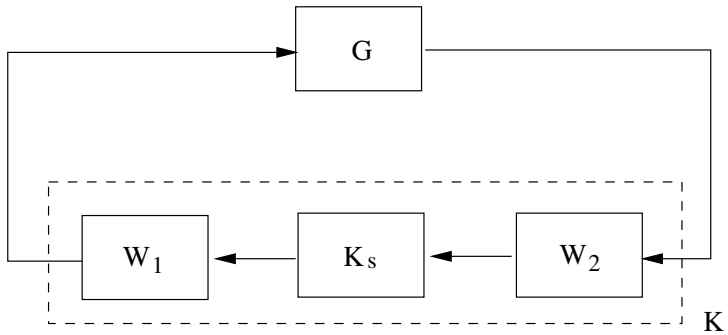


(b)

Fig 25 The Shaped Plant and Controller

Next the controller $K_S$ is synthesized by solving the robust stabilization problem (Section 4.2.2) for the shaped plant $G_S$ with a NLCF: $G_S = M^{-1}{}_S N_S$. Finally the feedback controller for the plant *G* is realized as $K = W_1 K_S W_2$ (see Fig. 25 (b)). Note that the maximum stability margin $\varepsilon_{\max}$ (Eq. (22)) indicates the magnitude of the maximum allowable perturbation of the shaped plant $G_S$. In this procedure, $\varepsilon_{\max}$ is treated as a design indicator of the proposed controller.

### 4.2.4Controller Synthesis and Simulation

As mentioned in Section 3.1.1, we will utilize the advantages of virtual-look-ahead methodology in the controller design. From Eq.(16) and Eq.(21), we can get the transfer function from the steering angle ( $\delta$ ) to the lateral error at the virtual sensor ( $y_s$ ) (define it as $G_P(s)$). The nominal operating condition is selected as $v$=18 m/s, $\mu$=0.8 and $m_2$=10670 kg. If we have a good inner-loop controller, the steering actuator can be modeled as a first-order dynamic system approximately (represent it as $G_A(s)$). The nominal plant $G(s)$ is defined as $G(s) = G_P(s)G_A(s)$. To avoid the chattering of the steering column generated by the fast-responding steering actuator (higher bandwidth compared to that of vehicle dynamics), a low-pass filter $W_2(s)$ is chosen to attenuate the noise :

$$W_2(s) = \frac{1}{5s+1}$$

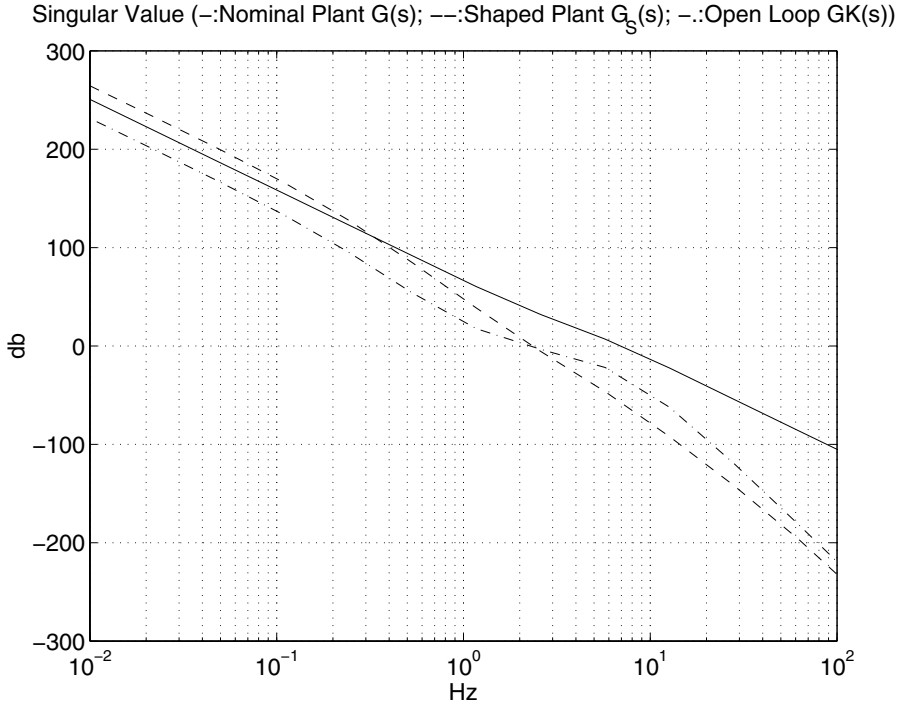


Fig 26 Singular values of the nominal plant $G(s)$ (--), the shaped plant $G_S(s)$ (- -) and the open-loop transfer function $GK(s)$ (**-.-.**)(with reduced-order controller)

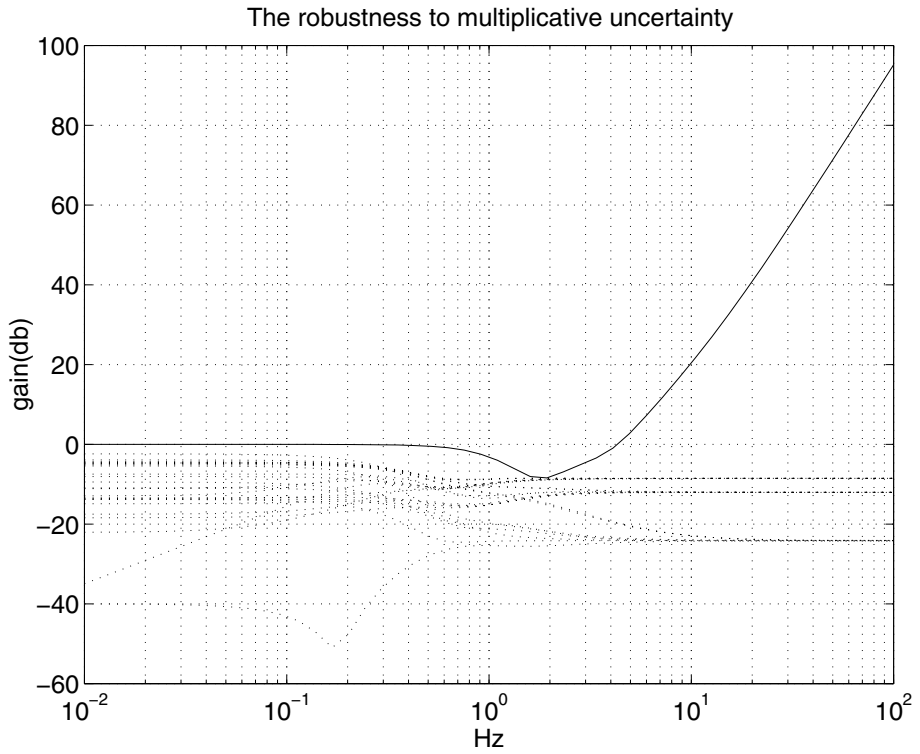


Figure 27 The maximum allowable multiplicative uncertainty (solid line) and multiplicative uncertainties caused by varying $v \in$ [0 25] m/s, $\mu \in [0.5 \quad 1]$ and $m_2 \in [5000 \quad 24000]$ kg

A constant gain 2 is chosen for $W_1(s)$ to obtain the desired small tracking error. Since windup may deteriorate the system performance, we do not put an integral action in $W_1(s)$ and $W_2(s)$. On the other hand, the H-infinity synthesized controller will have at least the same order as the shaped plant, thus the orders of the weighting filters should be kept as small as possible. In this case, the shaped plant $G_S(s)$ is eighth order and its singular value is shown in Fig.26. Applying above LSDP, we obtain a H-infinity loop shaping controller $K_s(s)$ with $\varepsilon_{\max}$ = 0.2053. After cascading the shaping filters, it becomes a ninth order controller. Using the balanced residualization method (Fernando and Nicholson, 1982), the order of *K*(*s*))is reduced to four. The singular values of open-loop transfer function *GK(s)* (with reduced controller *K*(*s*)) is also shown in Fig. 26. The maximum allowable multiplicative plant perturbation for closed-loop stability can be computed by $\frac{1}{\overline{\sigma}(GK(I-GK)^{-1})}$. As seen in Fig. 27, the multiplicative uncertainties (dotted line) caused by varying $v \in$ [0 to25] m/s, $\mu \in [0.5 \quad 1]$ and $m_2 \in$ [5000 24000] kg are smaller than the maximum allowable value (solid line).

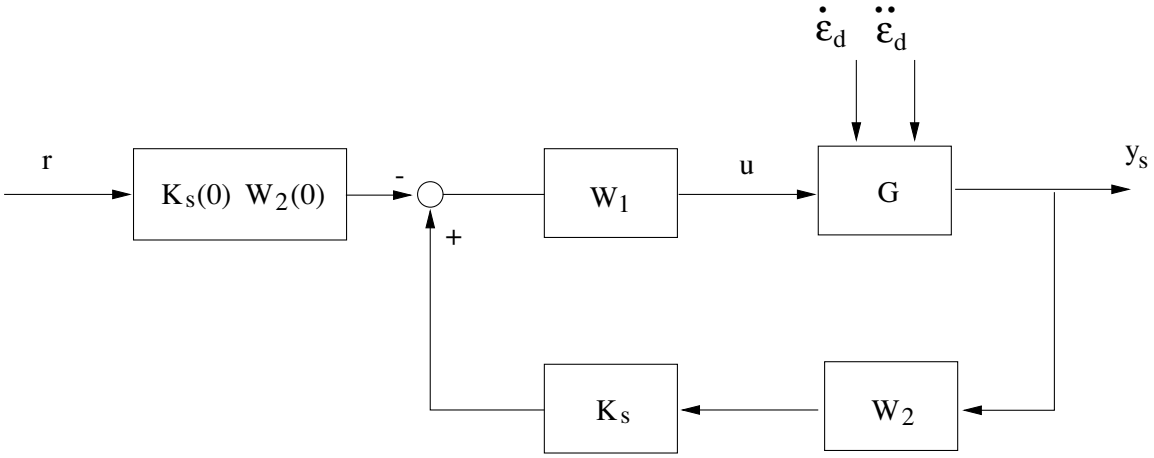

Figure 28 Implementation of the controller

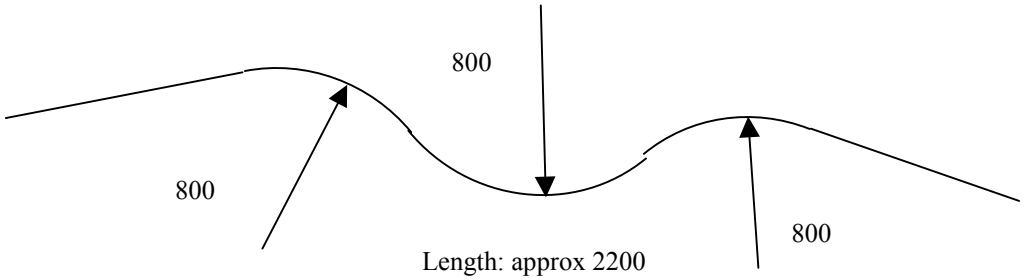

Figure 29 Crows Landing test site

The H-infinity loop shaping controller is implemented as shown in Fig. 28. The road curvature is treated as a disturbance to the plant $G$ by way of $\dot{\varepsilon}_d$ and $\ddot{\varepsilon}_d$. This configuration has some advantages over the conventional feedback control structure. For example, the reference does not directly excite the dynamics of $K_S(s)$, which may result in a larger overshoot. The constant prefilter ensures a steady-state gain of 1 between reference input r (desired look-ahead trajectory) and $y_s$. Here $r$ is set to be zero for regulation of $y_s$.

The scenario for numerical simulation is selected to follow the test track at the Crows Landing test site (Fig.29). Figure 30 shows the simulation results for the nominal condition and two perturbed conditions.

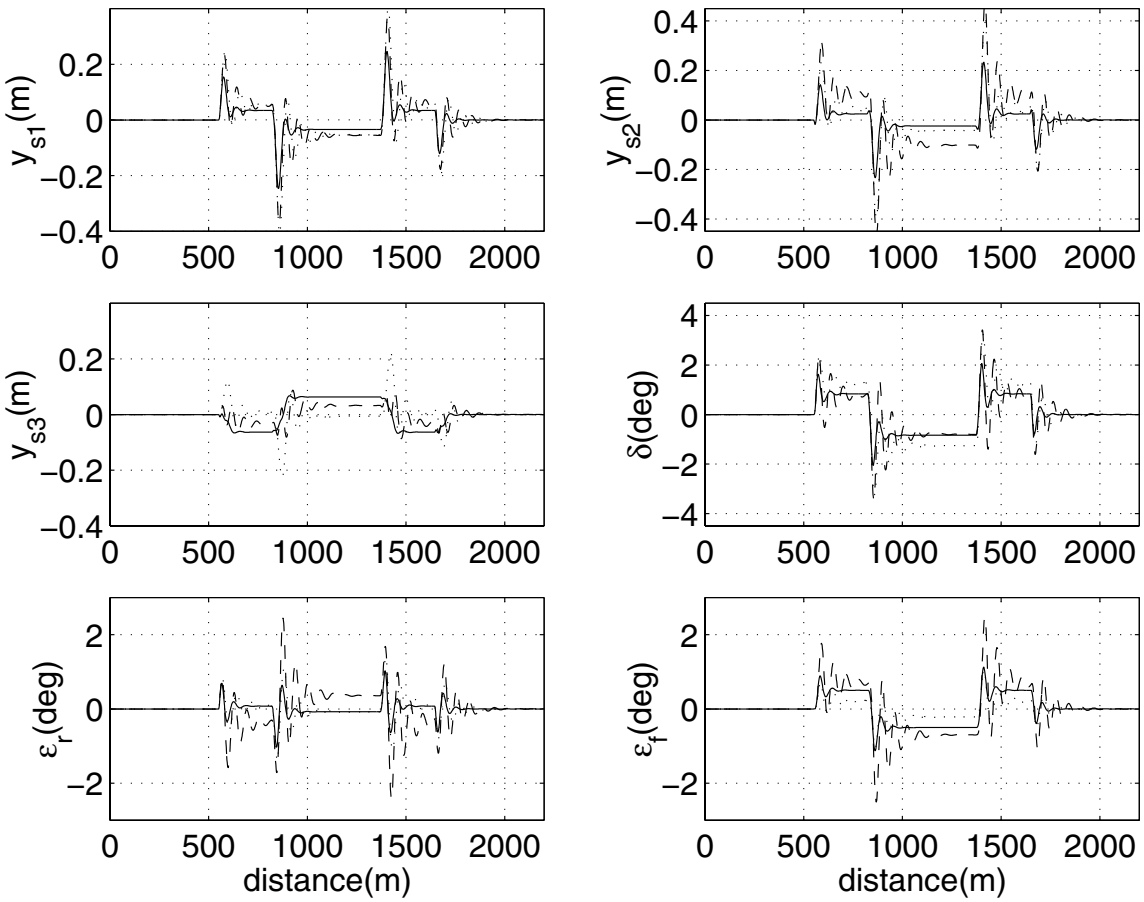


Figure 30 Closed-loop simulation: nominal condition (solid: v=18 m/s, $\mu$=1.0, $m_2$=23472 kg) and perturbed situations (dashed:$v$=25 m/s, $\mu$=0.8, $m_2$=24000 kg) (dashed line) and (dotted:$v$=20 m/s, $\mu$=0.6, $m_2$=5000 kg)

As seen from Fig. 30, the steady-state lateral errors at the tractor front axle ( $y_{s1}$ ), the tractor rear axle ( $y_{s2}$ ) and the trailer rear axle ( $y_{s3}$ ) are smaller than 0.1 m for the nominal condition and 0.2 m for perturbed conditions. However, the transient tracking errors can be as high as 0.45 m for perturbed conditions when entering curved sections at 825 m and 1375 m where the road curvature $\rho$ is changing from +/-1/800 m to -/+ 1/800 m. Steering actions are smooth both on curved and straight sections which can ensure driver comfort and the extended life of the steering actuator/column.

### 4.3 Sliding mode controller

The following subsections describe a nonlinear sliding mode controller design for lateral control of tractor semitrailers.

### 4.3.1 Model Reformulation

Let the generalized coordinate be $\dot{q} = [V_y, \dot{\varepsilon}_1, \dot{\varepsilon}_f]^T$, where $v_y$ is the lateral velocity, $\dot{\varepsilon}_1$ and $\dot{\varepsilon}_f$ are the tractor yaw rate and the trailer relative yaw rate respectively. Then, the simplified vehicle model with respect to the unsprung mass frame of the tractor is

$$M\ddot{q} + c(q, \dot{q}) = 2C_{\alpha f}(1 \quad l_f \quad 0)^T \delta \tag{25}$$

where, $\delta$ is the front wheel steering angle, $M$ is a 3x3 inertia matrix and $c$ is a 3x1 vector whose elements are functions of $q$, $\dot{q}$ and vehicle system parameters. Let the sensor location from the tractor's C.G. be $d_s$, then, the sensor output, i.e., the lateral error at the sensor position relative to the road center line is given by

$$y_s = y_r + d_s \varepsilon_r$$

Differentiating it, we obtain

$$\dot{y}_s = \dot{y}_r + d_s \dot{\varepsilon}_r$$

By noting $\dot{y}_r = V_y + V_x \varepsilon$, we get $\dot{y}_s = V_y + V_x \varepsilon_r + d_s \dot{\varepsilon}_r$. The highway road is designed to be a series of smooth connections of straight lines and arcs of constant radii. Thus under the assumption that the longitudinal velocity $V_x$ is constant, the desired yaw rate $\dot{\varepsilon}_d$ is constant on each road segment. Then,

$$\ddot{y}_s = \dot{V}_y + d_s \ddot{\varepsilon}_1 + V_x \dot{\varepsilon}_r \tag{26}$$

Note that the Eq. (25) represents three equations. By substituting the third equation to the first and second equations , we have

$$A\begin{pmatrix} \dot{V}_y \\ \ddot{\varepsilon}_1 \end{pmatrix} + b = 2C_{\alpha f}\begin{pmatrix} 1 \\ l_{f1} \end{pmatrix}\delta \tag{27}$$

where,

$$A = \begin{pmatrix} M_{11} - \frac{M_{13}}{M_{33}} M_{31} & M_{12} - \frac{M_{13}}{M_{33}} M_{32} \\ M_{21} - \frac{M_{23}}{M_{33}} M_{31} & M_{11} - \frac{M_{23}}{M_{33}} M_{32} \end{pmatrix}$$

$$b = \begin{pmatrix} c_1 - \frac{M_{13}}{M_{33}} c_3 \\ c_2 - \frac{M_{23}}{M_{33}} c_3 \end{pmatrix}$$

Let $F = A^{-1}$. Then

$$\dot{V}_y = F_{11}(2C_{\alpha f}\delta - b_1) + F_{12}(2C_{\alpha f} l_{f1}\delta - b_2) \qquad \ddot{\varepsilon}_1 = F_{21}(2C_{\alpha f}\delta - b_1) + F_{22}(2C_{\alpha f} l_{f1}\delta - b_2) \tag{28}$$

where $F_{ij}$ s are the i-j elements of $F$. Substituting Eq. (28) to Eq. (26), the error dynamics $\ddot{y}_s$ can be written as

$$\ddot{y}_s = b_x(q, \dot{q})\delta + f_x(q, \dot{q}) + \tilde{f}_x(q, \dot{q}) \tag{29}$$

where

$b_x(q, \dot{q}) = 2C_{\alpha f}\left[(F_{11} + d_s F_{21}) + (F_{12} + d_s F_{22}) l_{f1}\right]$ $f_x(q, \dot{q}) = -\left[(F_{11} + d_s F_{21}) b_1 + (F_{12} + d_s F_{22}) b_2\right] + V_x \dot{\varepsilon}_r$

and the extra term $\tilde{f}_x(q, \dot{q})$ has been added to represent all terms that can not be modeled exactly (e.g., the nonlinear components of tire model and external disturbances). The controller will be designed based on Eq. (29). Considering the physical properties of the system, the following reasonable assumptions are made.

**Assumption 1.** *The unknown nonlinear function* $\tilde{f}_x(q,\dot{q})$ *is bounded above by a known function,* $\alpha(q,\dot{q},t)$ *, i.e.,* $\left|\tilde{f}_x(q,\dot{q},t)\right| \le \alpha(q,\dot{q},t)$.

**Assumption 2.** $b_x(q,\dot{q})$ *is a positive function*.

Note that the first assumption is about the extent of model uncertainties. The second assumption is to ensure that the input gain in Eq. (29) is nonzero all the time. The objective is to design a SMC control law for $\delta$ such that the output $y_s$ will track the desired output trajectory $y_{s,desire}(t)$ as close as possible.

### 4.3.2Design of Sliding Mode Control

We see that the plant described by Eq. (29) has relative degree of two with respect to the given input-output pair $\delta$ and $y_s$. Let the sliding variable be defined as

$$s = \dot{e} + \lambda e \tag{30}$$

where $e = y_s - y_{s,desire}$ is the output tracking error and $\lambda$ is a positive constant. Then,

$$\begin{aligned} \dot{s} &= \ddot{e} + \lambda\dot{e} \\ &= \ddot{y}_s - \ddot{y}_d + \lambda\dot{e} \\ &= b_x\delta + f_x + \tilde{f}_x - \ddot{y}_d + \lambda\dot{e} \end{aligned} \tag{31}$$

Choose $\delta$ as

$$\delta = \frac{-1}{b_x}\left(f_x - \ddot{y}_d + \lambda\dot{e} + (\alpha + k)\,\mathrm{sgn}(s)\right) \tag{32}$$

where, $k$ is a design parameter and $\mathrm{sgn}(s)$ is a sign function, i.e. sgn($s$) = 1 for $s > 0$, = 0 for $s = 0$ and = 1 for $s > 0$.

Noting Assumption 1, Eq. (30) and Eq. (31) imply

$$\begin{aligned} s\dot{s} &= s\tilde{f}_x - \alpha|s| - k|s| \\ &\le -k|s| \end{aligned}$$

which forces the sliding variable $s$ go to zero within finite time, $s(t{=}0)/k$. Since Eq. (30) defines a stable system for $s = 0$, the output tracking error will also go to zero asymptotically. One undesired problem of this kind of control law is chattering caused by the sign function. Chattering can be eliminated by substituting the sign function with the saturation function, $sat(s/\Phi)$: $sat(s/\Phi) = -1$ for $s < -\Phi$, $= s/\Phi$ for $-\Phi \le s \le \Phi$ and $= 1$ for $s > \Phi$.The modified control law guarantee that the sliding surface reach the boundary of surface $s = 0$, the size of which is determined by $\Phi$.

### 4.3.3Simulation results of SMC

The simulation scenario for a tractor-semitrailer at a velocity of 60 *mph* is as follows. Initially the vehicle travels on a straight section for 1 second; at $t$ = 1 sec, it enters a curved section with a radius of 600 *m*; and at $t$ = 8 sec, it leaves the curved section and continue to run on a straight section.

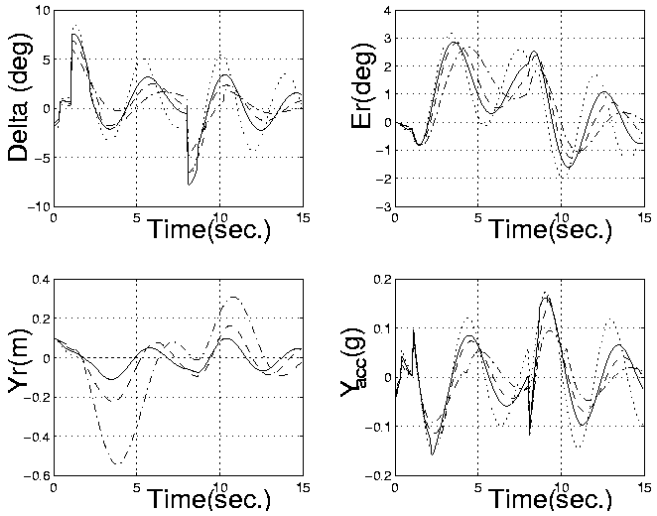


Fig. 31. Simulation of SMC for Different $d_s$: dotted($d_s$ = 0 *m*), solid($d_s$ = 3.5 *m*), dashed($d_s$ = 7 *m*), dashdot($d_s$ = 15 *m*)

Figure 31 shows the simulation results with unmodeled dynamics and different look ahead distances, but no parametric uncertainties. Four plots in the figure shows front wheel steering angle (Delta), tractor's yaw error (Er), lateral tracking error (Yr) and lateral acceleration (Y_acc) at the tractor's CG. They indicate the effect of the sensor location, which is consistent with the linear analysis by Wang and Tomizuka (1998). By increasing the look-ahead distance, the peak steering angle is reduced, tractor yaw rate and the acceleration becomes smoother. On the other hand, with the increase of the look-ahead distance, the lateral error at the tractor's CG is increased. This means, with only one control input (steering angle), we have to select look-ahead distance, which compromises the lateral tracking error and the performance.

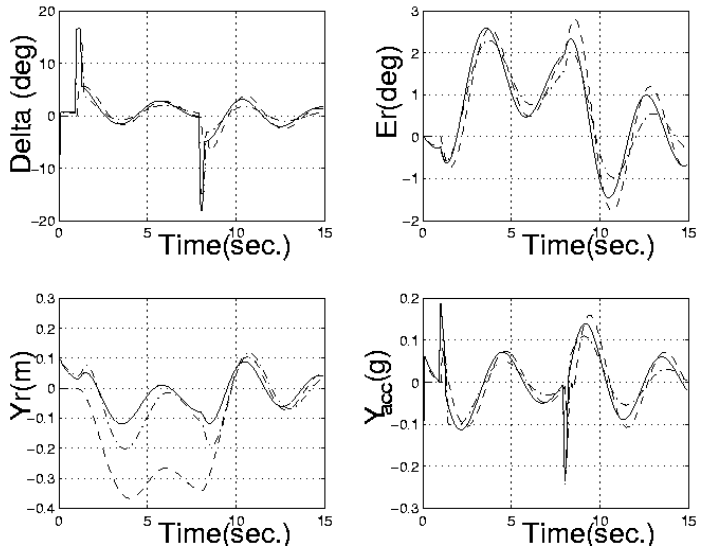


Fig. 32. SMC for 30% of Parametric Uncertainties:solid($d_s$ = 3.5 *m*, $\alpha$ = 6),

dashed($d_s = 3.5\ m,\ \alpha = 0.6$), dashdot($d_s = 7\ m,\ \alpha = 6$)

Figure 32 is the simulation result with 30% of parametric errors in the tire cornering stiffness. We can see that if the model parameters are not accurate, then both the lateral and yaw errors become larger with the same amount of steering input. In order to reduce the tracking errors, we have to lump the parametric uncertainties into the model uncertainty term in the SMC design, which enlarges $\alpha$ in Eq. (32) and inevitably results in a high gain controller. It also shows that with the larger $d_s$, even higher gain is expected to obtain the same level of tracking error. Furthermore, the convergence is significantly slowed down because the terms canceling the nonlinear dynamics in the SMC law are no longer appropriate. This motivates adaptive robust control.

## 5 Experimental Results

The linear controllers presented in the previous section were implemented on the test vehicle. The controllers were tested on a 2200m long test track at the Crow's Landing test facility (see Fig. 29). The test conditions were dry pavement with no wind.

### 5.1 Results of the loop shaped controller

Speeds of up to 45 miles per hour for curve transitions of +800 to –800 meters were achieved with this controller. The maximum speed achieved on the straight sections of the track was 60 mph. The tracking achieved by this controller is shown in Fig. 33. The top graph is a plot of vehicle speed v/s time. The bottom graph is the corresponding lateral error as measured by magnetometers at the front end of the tractor. The steering action was smooth and the trailer dynamics were well damped. However, the performance during curve transitions was not satisfactory.

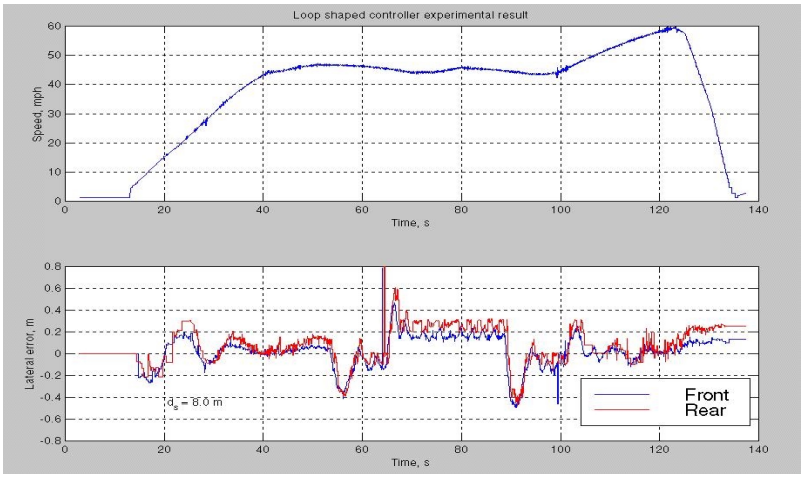


Fig. 33 Closed experiment using linear loop shaping controller

Further tuning of the controller parameters may enhance the performance. However, it may be more beneficial to consider the relative yaw and the lateral error as separate inputs to the controller. This aspect will be investigated.

### 5.2 H-infinity loop shaped controller

The initial results were encouraging and correlated with simulation results well. Experimental results are shown in Fig.34 and Fig. 35.

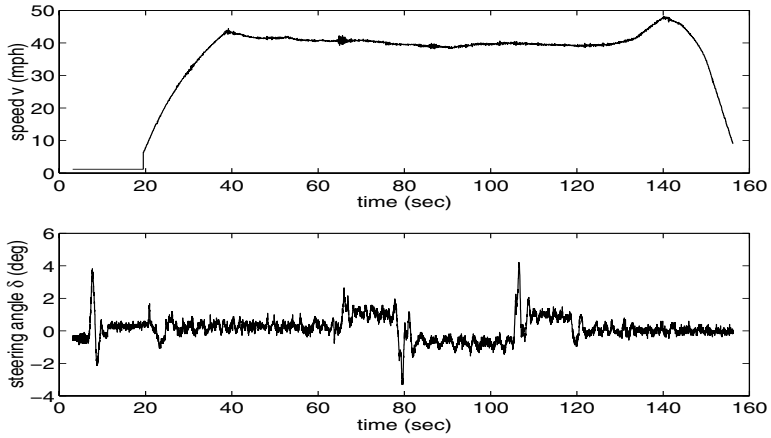


Figure 34 Vehicle longitudinal speed $v$ (mph) (up) and steering angle $\delta$ (deg)

Figure 34 shows the vehicle speed and the front wheel steering angle when the test vehicle was driven along the test track (Fig.29) under closed loop steering control. The speed was manually adjusted not to exceed 50 mph (upper plot in Fig.34). Large excursions of the steering angle when the vehicle arrives at points where the road curvature changes (lower plot in Fig.34) are consistent with the simulation results in the previous section (see Fig. 30). Some noise signal is apparent in the plot of the steering angle, which is attributed to the vibration of the potentiometer placed close to the ground. In fact, the motion of the hand wheel was observed to be smooth.

As shown in Fig. 35, steady-state tracking errors of the tractor ( $y_{s1}$ and $y_{s2}$ ) are small on both straight road sections (<0.15 m) and curved road sections (<0.2 m). The off-tracking error is small at the rear axle of the trailer ( $y_{s3}$ <0.2 m).

This preliminary experiment validates the feasibility of the proposed controller which is robust under test speeds up to 45 mph.

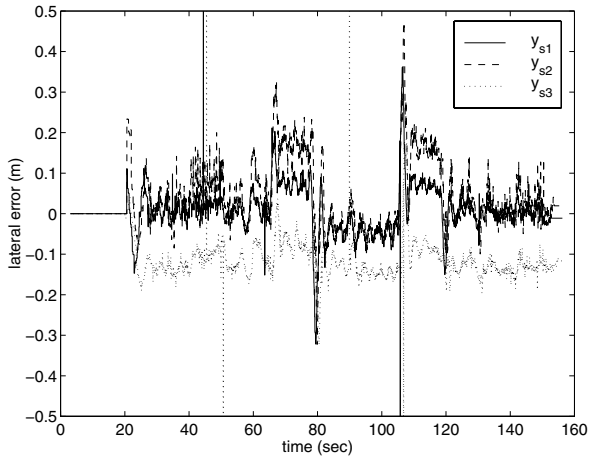


Figure 35 Lateral tracking error (m): lateral error at the tractor front axle ( $y_{s1}$ ); lateral error at the tractor rear axle ( $y_{s2}$ ); lateral error at the trailer rear axle ( $y_{s3}$ )

## 6 Conclusions

Experimental aspects of the PATH's research on the lateral control of heavy vehicles have been presented. The experimental vehicle (Freightliner tractor with a 45' semitrailer) is fully equipped with all the necessary sensors and actuators for experiments. Open loop tests validated the previously derived dynamic model of the tractor-semitrailer heavy vehicle at speeds upto 60 miles per hour and at frequencies up to 1 Hz. Test results also showed the discrepancy from the linear simplified model at higher frequencies, which is attributed to the nonlinear dynamics of the vehicle. The nonlinear dynamics make the control of heavy vehicles challenging, and it has been and will be addressed in our research. Three controller designs, one based on classical loop shaping, one based on the $H_\infty$ optimal loop shaping and a robust sliding mode controller was presented. Among the three controllers, linear robust controllers were successfully tested at the velocity up to 45mph on the test track at Crows Landing. The experimental validation has so far been limited to dry road surface, no wind disturbances and minimal cargo loading. The performance of the linear controller under these ideal conditions will be used as the baseline in our further research, the emphases of which include 1) evaluation of existing and new controllers under the ideal conditions by experiments, 2) evaluation of linear and nonlinear controllers on slippery road surface, under influence of cross wind and varying cargo loads by simulations and experiments, and 3) usage of the brake actuator and the inertia sensors (gyroscopes and accelerometers) for enhanced control performance.

ACKNOWLEDGEMENT

This work was sponsored by California PATH program. The contents of this report reflect the views of the authors who are responsible for the facts and the accuracy of the data presented herein. The contents do not necessarily reflect the official views or policies of the state of California. This report does not constitute a standard, specification, or regulation. We also acknowledge the technical contributions of Dr. C. Chen, D. de Bruin, F. Bonnay, D. Nelson, P. Kretz, H.-S. Tan and W-B. Zhang.

**References**

Ashmore, C. and T. Mitchell (1997). WesTrack: Putting ITS to Work, *Public Roads,* July/August, 8-15.

Bishel, R. (1993). Dual-Mode Truck: Automated and Manual Operation, SAE *technical paper series, no. 931837.*

Bruin, de D. and P. van den Bosch (1998). Modelling a double articulated vehicle with four steerable axes, *Report,* Department of Electrical Engineering, Eindhoven University of Technology, Netherlands.

Chen, C. and M. Tomizuka (1995a). Dynamic Modeling of Articulated Vehicle for Automated Highway Systems, *Proceedings of the American Control Conference*, 653-657.

Chen, C. and M. Tomizuka (1995b). Steering and Independent Braking Control of Tractor-semitrailer Vehicle in Automated Highway Systems. *Proc. of IEEE Conference on Decision and Control*, New Orleans, 1561-1566.

Chen. C. and M. Tomizuka, (1996) "Lateral Control of Tractor Semitrailers for Automated Highway Systems", PATH Research Report no UCB-ITS-PRR-96-33, California PATH, UC Berkeley, CA.

Chen, C. (1996), "Backstepping Design of Nonlinear Systems and Its Application to Vehicle Latreal Control in Automated Highway Systems", PhD Thesis, UC Berkeley, CA.

Daimler Benz (1998), One driver, Two Trucks, *Hightech Report '98,* 82-83.

Enkür, E. (1998). Lateral MOMO-control of bus, *M. Sc. Thesis*, Department of Electrical Engineering of the Eindhoven University of Technology, Netherlands.

Fenton , R., Melocik, G.C. and Olson, K.W. , June1976, “On Steering of Automated Vehicles: Theory and Experiment,” IEEE Transactions on Automatic Control, vol. AC-21, no. 3 pp

Fernando and H. Nicholson, (1982), ``Singular Perturbational Model Reduction of Balanced Systems", *IEEE Trans. on Automatic Control* AC-27(2):466-468.

M. Fujita, K. Hatake, F. Matsumura and K. Uchida, (1993), ``Experiments on the Loop Shaping Based H-infinity Control of a Magnetic Bearing", *Proc. of American Control Conference*, San Francisco, pp.8-12.

Gardels , K., 1960, “Automatic Car Controls for Automated Highways”, GMR, General Motor Corporation, Warren, MI, Report, GMR-276.

Hingwe, P. and M. Tomizuka (1998). A Variable Look-ahead Controller for Lateral Guidance of Vehicles, *Proceedings of the American Control Conference*, 31-35.

R. A. Hyde, (1991), ``The Application of Robust Control to VSTOL Aircraft", PhD thesis, University of Cambridge.

S. Mammar, (1996), ``H-infinity Robust Automatic Steering of a Vehicle", *Proc. of IEEE Intelligent Vehicle Symposium*, Piscataway, NJ, pp.19-24.

Mahrt R, (1992)., "Principles of Automatic Guidance of Vehicles on a Lane by Means of Permanent Magnet Nails and On-Board Computer Control," 21st Annual Conference on Vehicle Technology Group, IEEE, Washington, DC, 1992.

D. McFarlane and K. Glover, (1998),``Robust Control Design Using Normalized Coprime Factor Plant Description", *vol.138 of Lecture Notes in Control and Information Sciences*, Spring-Verlag.

R.T. O'Brien, P. A. Iglesias, and T. J. Urban, (1996), `` Vehicle Lateral Control for Automated Highway System", *IEEE Trans. on Control System Technology*, vol.4, no.3, pp.266-273.S.

Patwardhan, H.-S. Tan, and J. Guldner, (1997) ``A general Framework for Automatic Steering Control: System Analysis", *Proc. of American Control Conference*, Albuquerque, New Mexico, pp.1598-1602.

I. Postlethwaite and D. J. Walker, (1992), ``Advanced Control of High Performance Rotorcraft", Institute of Mathematics and Its Applications Conference on Aerospace Vehicle Dynamics and Control, Cranfield Institute of Technology, pp.615-619.

J. Sefton and K. Glover, (1990),``Pole-Zero Cancellations in the general H-infinity problem with reference to a two block design", *Syst. Contr. Lett*., vol.14, pp.295-306.

Tai, M. and M. Tomizuka (1998). Dynamic Modeling of Multi-Unit Heavy Vehicles. *International Mechanical Engineering Congress and Exposition, ASME Symposium on Transportation Systems*, 673-680.

Tai, M. and M. Tomizuka (1999). Robust Lateral Control of Heavy Vehicles for AHS, To be presented at *the 1999 IFAC World Congress*, Beijing, 1999.

M. Tsai, E. Geddes and I. Postlethwaite K, (1992), ``Pole-Zero Cancellations and Closed-Loop Properties of An H-infinity Mixed Sensitivity Design Problem", *Automatica* 3:519-530.

Varaiya, P. (1993). Smart Cars on Smart Road: Problems of Control, IEEE Trans. On AC, Vol. 38, No. 2, 195-207.

Wang, J.-Y. and M. Tomizuka (1998). Analysis and Controller Design Based on Linear Model for Heavy-Duty Vehicles, *International Mechanical Engineering Congress and Exposition, ASME Symposium on Transportation Systems*, Anaheim, CA.pp.729-735.

Wang, J.-Y. and M. Tomizuka (1999). Robust $H_\infty$ Lateral Control of Heavy-Duty Vehicles in the Automated Highway System. To be presented in *Proc. of American Control Conference*, San Diego.

Zhang, W.B.; Parsons, R.E.; West, T., 1990, “An intelligent roadway reference system for vehicle lateral guidance/control”, Proceedings of the American Control Conference, Vol. 1, pp. 281-286.

APPENDIX A

The linear lateral dynamics model of tractor-semitrailer is given by.

$$M\ddot{q} + D\dot{q} + Kq = F\delta + E_1\dot{\varepsilon}_d + E_2\ddot{\varepsilon}_d$$

where

$$q = \begin{bmatrix} y_r & \varepsilon_r & \varepsilon_f \end{bmatrix}^T$$

$$M = \begin{bmatrix} (m_1 + m_2) & -m_2(d_1 + d_3) & -m_2 d_3 \\ -m_2(d_1 + d_3) & I_{z1} + I_{z2} + m_2(d_1 + d_3)(d_1 + d_3) & I_{z2} + m_2 d_3 d_3 + m_2 d_1 d_3 \\ -m_2 d_3 & I_{z2} + m_2 d_3 d_3 + m_2 d_1 d_3 & I_{z2} + m_2 d_3 d_3 \end{bmatrix}$$

$$D = \frac{2}{v}\begin{bmatrix} (C_{\alpha f} + C_{\alpha r} + C_{\alpha t}) & l_1 C_{\alpha f} - l_2 C_{\alpha r} - (l_3 + d_1) C_{\alpha t} & -l_3 C_{\alpha t} \\ l_1 C_{\alpha f} - l_2 C_{\alpha r} - (l_3 + d_1) C_{\alpha t} & l_1^2 C_{\alpha f} + l_2^2 C_{\alpha r} + (l_3 + d_1)^2 C_{\alpha t} & l_3(l_3 + d_1) C_{\alpha t} \\ -l_3 C_{\alpha t} & l_3(l_3 + d_1) C_{\alpha t} & l_3^2 C_{\alpha t} \end{bmatrix}$$

$$K = 2\begin{bmatrix} 0 & -(C_{\alpha f} + C_{\alpha r} + C_{\alpha t}) & -C_{\alpha t} \\ 0 & -(l_1 C_{\alpha f} - l_2 C_{\alpha r} - (l_3 + d_1) C_{\alpha t}) & (l_3 + d_1) C_{\alpha t} \\ 0 & l_3 C_{\alpha t} & l_3 C_{\alpha t} \end{bmatrix}$$

$$F = 2C_{\alpha f}\begin{bmatrix} 1 \\ l_1 \\ 0 \end{bmatrix}$$

$$E_1 = \begin{bmatrix} -(m_1 + m_2)V - \frac{2}{V}(l_1 C_{\alpha f} - l_2 C_{\alpha r} - (l_3 + d_1) C_{\alpha t}) \\ m_2(d_1 + d_3)V - \frac{2}{V}(l_1^2 C_{\alpha f} + l_2^2 C_{\alpha r} + (d_1 + l_3)^2 C_{\alpha t}) \\ m_2 d_3 V - \frac{2}{V} l_3(l_3 + d_1) C_{\alpha t} \end{bmatrix}$$

$$E_2 = \begin{bmatrix} m_2(d_1 + d_3) \\ -(I_{z1} + I_{z2} m_2(d_1 + d_3)^2) \\ -(I_{z2} + m_2 d_3^2 + m_2 d_1 d_3) \end{bmatrix}$$

The parameter values are given in Table A1

| | | |
|---|---|---|
| $m_1$ | Mass of the tractor | 7,700 kg |
| $m_2$ | Mass of the trailer | 10,500 kg |
| $I_{z1}$ | Yaw moment of inertia of the tractor | 46,000 kgm*m |
| $I_{z2}$ | Yaw moment of inertia of the trailer | 162,000 kgm*m |
| $l_1$ | Distance of the front axle from the tractor center of gravity | 1.65 m |
| $l_2$ | Distance of the rear axle from tractor center of gravity | 3.745 m |
| $l_3$ | Distance of the trailer axle form the fifth wheel | 6.5 m |
| $d_1$ | Distance of the fifth wheel from the tractor center of gravity | 3.245 m |
| $d_3$ | Distance of the trailer center of gravity form the fifth wheel | 3.805 m |
| $C_{\alpha f}$ | Cornering stiffness of the front tires | 180,430 N/rad |
| $C_{\alpha r}$ | Cornering stiffness of the rear tires | 324,744 N/rad |
| $C_{\alpha t}$ | Cornering stiffness of the trailer tires | 324,744 N/rad |

Table A1. Parameter values for the tractor semitrailer model.